Taylor & Francis
Taylor & Francis Group

Journal of Enzyme Inhibition and Medicinal Chemistry

ISSN: (Print) (Online) Journal homepage: www.tandfonline.com/journals/ienz20

Dependence on linkers' flexibility designed for benzenesulfonamides targeting discovery of novel hCA IX inhibitors as potent anticancer agents

Haytham O. Tawfik, Amany Belal, Mohammed A. S. Abourehab, Andrea Angeli, Alessandro Bonardi, Claudiu T. Supuran & Mervat H. El-Hamamsy

To cite this article: Haytham O. Tawfik, Amany Belal, Mohammed A. S. Abourehab, Andrea Angeli, Alessandro Bonardi, Claudiu T. Supuran & Mervat H. El-Hamamsy (2022) Dependence on linkers' flexibility designed for benzenesulfonamides targeting discovery of novel hCA IX inhibitors as potent anticancer agents, Journal of Enzyme Inhibition and Medicinal Chemistry, 37:1, 2765-2785, DOI: 10.1080/14756366.2022.2130285

To link to this article: https://doi.org/10.1080/14756366.2022.2130285

JOURNAL OF ENZYME INHIBITION AND MEDICINAL CHEMISTRY
2022, VOL. 37, NO. 1, 2765–2785
https://doi.org/10.1080/14756366.2022.2130285

Taylor & Francis
Taylor & Francis Group

RESEARCH PAPER

OPEN ACCESS Check for updates

Dependence on linkers' flexibility designed for benzenesulfonamides targeting discovery of novel hCA IX inhibitors as potent anticancer agents

Haytham O. Tawfik[a], Amany Belal[b,c], Mohammed A. S. Abourehab[d,e], Andrea Angeli[f], Alessandro Bonardi[f], Claudiu T. Supuran[f] and Mervat H. El-Hamamsy[a]

[a]Department of Pharmaceutical Chemistry, Faculty of Pharmacy, Tanta University, Tanta, Egypt; [b]Medicinal Chemistry Department, Faculty of Pharmacy, Beni-Suef University, Beni-Suef, Egypt; [c]Department of Pharmaceutical Chemistry, College of Pharmacy, Taif University, Taif, Saudi Arabia; [d]Department of Pharmaceutics, Faculty of Pharmacy, Umm Al-Qura University, Makkah, Saudi Arabia; [e]Department of Pharmaceutics and Industrial Pharmacy, College of Pharmacy, Minia University, Minia, Egypt; [f]Department of NEUROFARBA, Section of Pharmaceutical and Nutraceutical Sciences, University of Florence, Sesto Fiorentino, Italy

ABSTRACT

Herein we reported the design and synthesis of two series comprising twenty-two benzenesulfonamides that integrate the *s*-triazine moiety. Target compounds successfully suppressed the hCA IX, with IC_{50} ranging from 28.6 to 871 nM. Compounds **5d**, **11b**, **5b**, and **7b** were the most active analogues, which inhibited hCA IX isoform in the low nanomolar range (K_I = 28.6, 31.9, 33.4, and 36.6 nM, respectively). Furthermore, they were assessed for their cytotoxic activity against a panel of 60 cancer cell lines following US-NCI protocol. According to five-dose assay, **13c** showed significant anticancer activity than **5c** with GI_{50}-MID values of 25.08 and 189.01 μM, respectively. Additionally, **13c**'s effects on wound healing, cell cycle disruption, and apoptosis induction in NCI-H460 cancer cells were examined. Further, docking studies combined with molecular dynamic simulation showed a stable complex with high binding affinity of **5d** to hCA IX, exploiting a favourable H-bond and lipophilic interactions.

HIGHLIGHTS

- Carbonic anhydrase (CA) inhibitors comprising rigid and flexible linkers were developed.
- Compound **5d** is the most potent CA IX inhibitor in the study (IC50: 28.6 nM).
- Compounds **5c** and **13c** displayed the greatest antiproliferative activity towards 60 cell lines.
- Compound **13c** exposed constructive outcomes on normal cell lines, metastasis, and wound healing.
- Molecular docking and molecular dynamics (MDs) simulation was utilised to study binding mode.

GRAPHICAL ABSTRACT

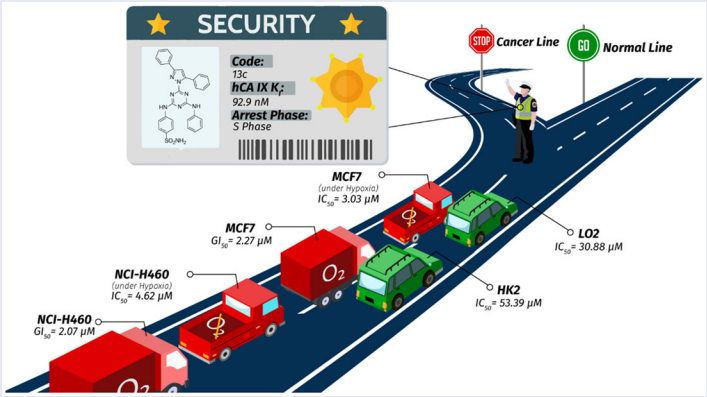

ARTICLE HISTORY

Received 4 September 2022
Revised 21 September 2022
Accepted 22 September 2022

KEYWORDS

CA inhibitors; linkers flexibility; colony formation; wound healing; molecular dynamics

CONTACT H. O. Tawfik haytham.omar.mahmoud@pharm.tanta.edu.eg Department of Pharmaceutical Chemistry, Faculty of Pharmacy, Tanta University, Tanta, Egypt; C. T. Supuran claudiu.supuran@unifi.it Department of NEUROFARBA, Section of Pharmaceutical and Nutraceutical Sciences, University of Florence, Sesto Fiorentino, Italy

Supplemental data for this article is available online at https://doi.org/10.1080/14756366.2022.2130285.

Introduction

The carbonic anhydrase (CA) enzymes are zinc-metalloenzymes family that catalyse the conversion of CO_2 and H_2O to the dissociated products of H_2CO_3 (HCO_3^- and H^+ ions) reversibly in all organisms.[1,2] In humans, there are 15 distinct CA isoforms, each with its own molecular features, subcellular localisation, and tissue distribution.[3,4] These enzymes are required for a variety of physiological and cellular activities, including electrolyte secretion, acid–base balance, carbon dioxide transport, and biosynthetic pathways.[5,6] Compared to normal tissues, where CA IX expression is modest, the variety of solid tumours have some of the most overexpressed transmembrane proteins.[7,8] CA IX is used by tumour cells to keep the tumour microenvironment acidic, preventing tumour hypoxia-related responses and assisting tumour cell survival and proliferation.[9] CA IX's overexpression in tumour cells made it an ideal candidate as a viable target for developing novel small compounds for both tumour diagnostics and treatments.[10] Many selective CA IX inhibitors have recently been described in the literature, which are in various stages of clinical trials and have shown good activity against different types of solid tumours.[11] The sulphonamide derivative SLC-0111, an efficient inhibitor of CA IX and CA XII, which was advanced in subsequent clinical investigations, is a well-known selective anticancer drug candidate.[12] The well-known tail approach was used to develop SLC-0111, which includes a ureido linker between the zinc-binding group (ZBG) benzenesulfonamide and the tail of the inhibitor. The tail portion of the inhibitor, which offers isoenzyme specificity over off-target isoenzymes, is made more flexible by the linker moiety to engage with the individual amino acid residues on the active site.[13] There are several bioisosteric groups reported exchanging urea as a tailing linker in various benzenesulfonamide derivatives, which is the most effective class of CA inhibitors.

Hydrazones are an important family of compounds because of their flexibility and structural similarities to a variety of biologically important natural chemicals.[14,15] The imine (N = C) group in hydrazone derivatives plays an important role in the mechanism of transformation and racemisation in biological systems[16,17] in addition to its chemical stability towards liver microsomal enzymes.[18,19] Reported CAs inhibitors having aforesaid chemical features are illustrated in Figure 1. In previous studies, isatin, phenyl, or pyrazole-moieties (**I**–**III**) that carry aromatic sulphonamides *via* hydrazone linker were declared as potent inhibitors of cancer-related hCA IX isoenzyme with the hCA IX K_Is values of 8.3 nM,[20] 14.6 nM,[21] and 19.7 nM,[22] respectively (Figure 1). Numerous studies and experiences pointed out that heterocyclic rings, such as pyrazoline **IV**, pyrazole **V**, and triazole **VI** bearing benzenesulfonamides are an attractive group of compounds with significant CAs inhibitory activity profiles towards CA IX isoform with K_Is values of 5.5 nM,[23] 302 nM,[24] and 180 nM,[25] respectively (Figure 1). In previous studies reported by our group,[26] compound **1** was considered a cornerstone to which any part of the above can be added to design more potent and selective inhibitors. Therefore, we have designed series **I** (**3a–c**, **5a–d,** and **7a–e**), having the hydrazone linker while in Series **II** (**9**, **11a,b**, **13a–e**, and **15a,b**), we have fixed the configuration of the hydrazone linker *via* incorporation in five-membered heterocyclic rings seeking to solve dilemma of hCA IX selectivity. Moreover, benzenesulfonamide was retained as a zinc-binding group in target compounds for Series **I** and **II**. Different lipophilic tails were constructed in Series **I** such as substituted isatins (**3a–c),** substituted benzenes **(5a–d),** and substituted phenylpyrazoles **(7a–e)**. Regarding Series **II**, the lipophilic tails were designed to be substituted pyrazolidines (**9 and 11a,b**), substituted pyrazoles (**13a–e**), and substituted triazoles (**15a,b**).

Results and discussion

Chemistry

New *s*-triazine-based benzenesulfonamide derivatives **3a–c**, **5a–d**, **7a–e**, **9**, **11a**,**b**, **13a–e**, and **15a**,**b** were synthesised by the chronological reactions sequence depicted in Schemes 1 and 2. The hydrazine derivative **1** was reacted with selected reagents to install a variety of phenyl or heterocyclic moieties connected to the *s*-triazine scaffold. Reaction of **1** with isatin derivatives **2a–c** in hot, dry methanol and glacial acetic acid as catalyst yielded **3a–c** (Scheme 1). The analogues **3a–c** may exist as the *Z*- or *E*-isomer relying on several factors which estimate the preferred configuration.[27] The development of a single stereoisomer was established by the ^{1}H NMR spectra of the compounds **3a** and **3b**. ^{1}H NMR of **3a** displayed a singlet at δ 10.68 ppm for the introduced NH of hydrazone moiety as an *E*-configured structure.[28] The downfield shift of the NH proton peak of isatin as in **3b**, which appears at 12.74 ppm, suggests that the NH proton of the hydrazone moiety is intramolecularly hydrogen-bonded with the carbonyl group of the indolinone ring, which resulted in the construction of the pseudo-six-membered ring as *Z*-configured structure[29] as shown in Figure 2.

Hydrazones **5a–d** and **7a–e** were easily synthesised in high yields (≥70%) by condensing equimolar amounts of **1** with different carbonyl compounds in boiling absolute MeOH. The geometry of target hydrazones **5a–c** and **7a–e** was considered as *E* isomers rather than *Z* isomers depending on ^{1}H NMR spectra that were assigned for the methine proton (=CH) between 8.07 and 8.35 ppm,[30] in addition to our reported results of NOESY study.[26]

Reagents and conditions: (**i**) Dry MeOH, *gl.* AcOH, reflux 25 h, (**ii**) Dry MeOH, *gl.* AcOH, reflux 5 h.

In Scheme 2, the hydrazinyl derivative **1** reacted, under neutral conditions, with the different active methylene compounds, namely ethyl cyanoacetate and dicarbonyl ketones, to afford products **9** and **13a–e,** respectively, in good yields. The target compounds **11a,b** were obtained through a cyclocondensation reaction of the corresponding hydrazino-triazine derivative **1** and the appropriate propenones, **10a,b** in absolute methanol and potassium hydroxide. Furthermore, the triazolotriazine derivatives **15a,b** were successfully synthesised by heating the hydrazine **1** in pyridine with either ethyl chloroformate to give **15a** or carbon disulphide to give **15b**. In the case of compound **15b**, duplication of the signals in its ^{1}H NMR spectrum was detected, even though only one spot in different TLC eluents was observed, which proves the presence of two isomers (depending on the position of nitrogen of the triazine ring that can be cyclised with carbon disulphide in basic medium). The proportion of the two isomers in this mixture, as indicated by ^{1}H NMR, was 1: 1 approximately. In addition, the absence of symmetrical exchangeable singlets protons after the addition D_2O at (10.02 and 10.23) and (12.60 and 12.82) ppm were assigned for two protons of NH of each isomer.

Furthermore, the lack of exchangeable singlets of D_2O at 7.29 and 14.17 ppm were assigned for SO_2NH_2 and SH protons, respectively, of each isomer. All of that indicates the presence of another isomer (Figure S1, see Supporting information). The presence of the two isomers was also confirmed using HPLC due to the presence of a twin peak at 6.734 and 7.666 min (Figure S2, see Supporting information). The two proposed isomers of compound **15b,** when refluxed with CS_2 in pyridine, are shown in Scheme 3, and the plausible mechanism of the formation of one of two isomers of compound **15b** is shown in Scheme 4.[31,32]

Reagents and conditions: (**i**) *gl.* AcOH, reflux 36 h; (**ii**) KOH, abs. MeOH, reflux 72 h; (**iii**) abs. MeOH, reflux 5 h; (**iv**) Ethyl

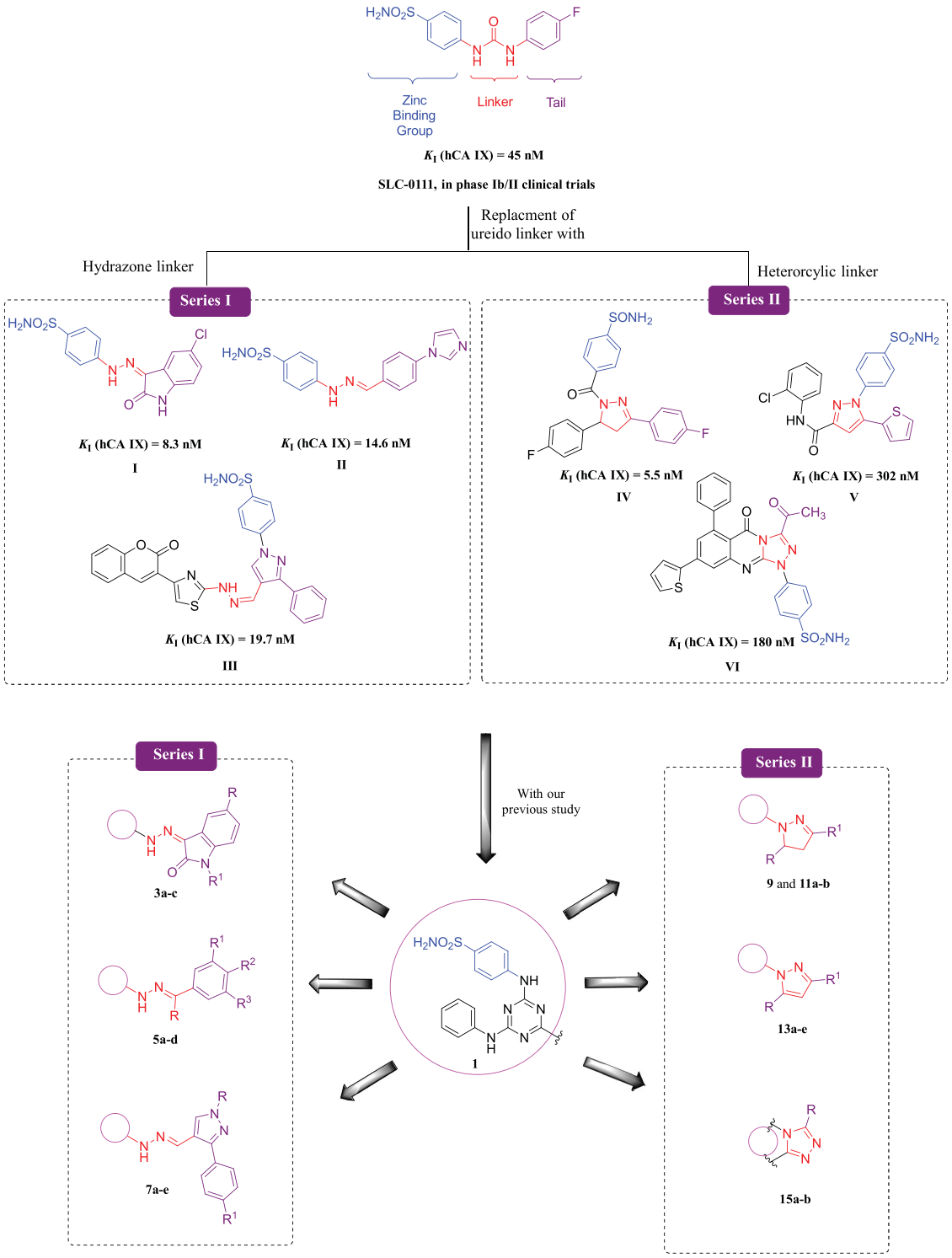

Figure 1. Structures of SLC-0111, some reported CAIs **I–VI** and design of target sulphonamides, Series **I** (**3a–c**, **5a–d**, and **7a–e**) and Series **II** (**9**, **11a,b**, **13a–e**, and **15a,b**).

chloroformate (for compound **15a**) or CS_2 (for compound **15b**), pyridine, reflux 16 h.

Twenty-two new compounds were designed and synthesised in this study. Their chemical structures were confirmed using ^1H, ^{13}C NMR, and EI-MS. Spectra are in the Supplementary file. In addition to elemental analysis results, the molecular ion peaks were in good harmony with the target compounds' molecular formula within the permitted range (±0.4). Some representative compounds were also measured their purity by HPLC (Agilent Technologies, Santa Clara, CA).

Biological evaluation

Carbonic anhydrase isoforms inhibition assay

Potency parameter. The four pharmacologically and physiologically significant CA isoforms, including the hCA I and II (cytosolic

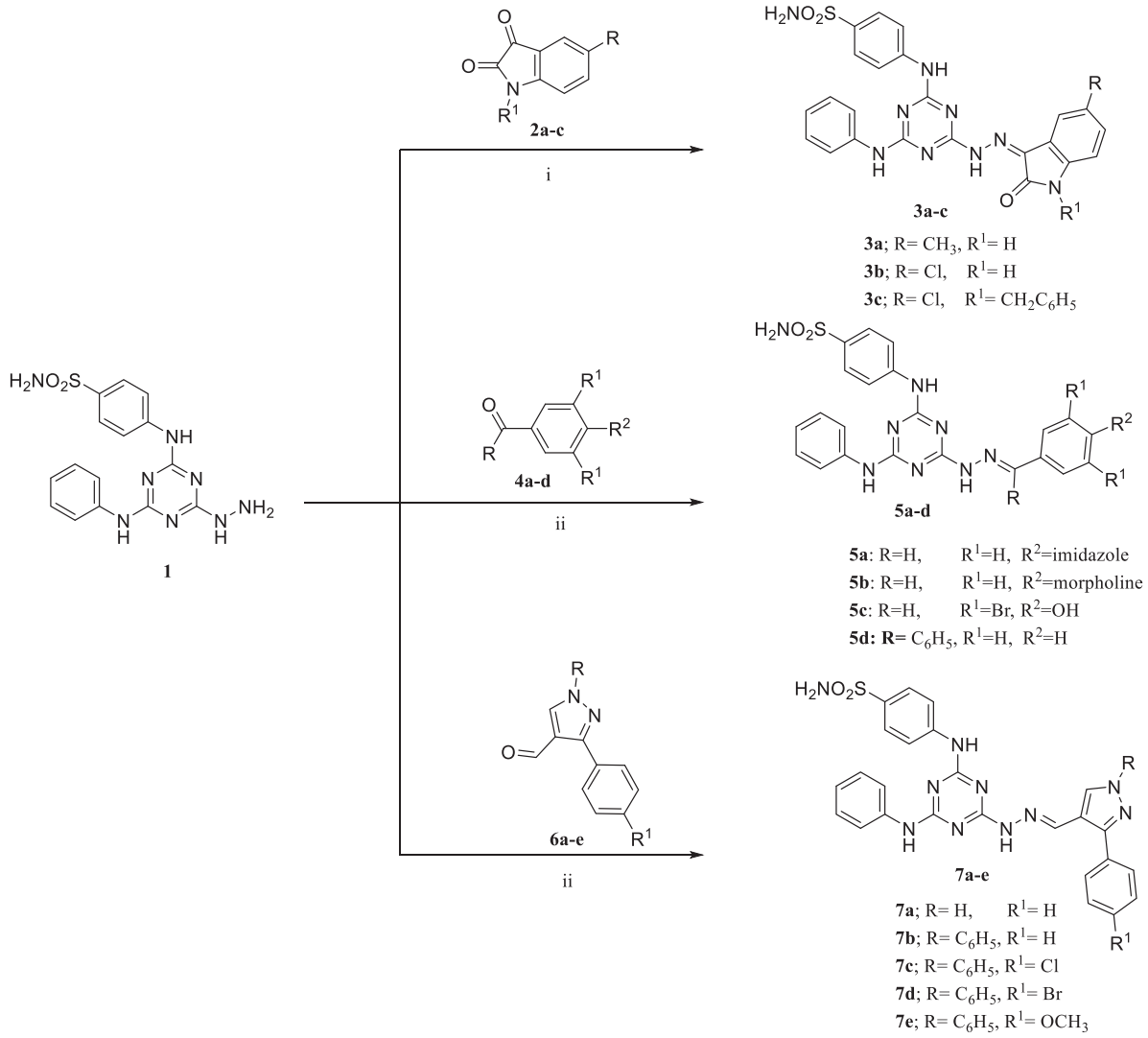

Scheme 1. Synthetic pathway of new sulphonamides analogues **3a–c**, **5a–d,** and **7a–e.**

isoforms) and the hCA IX and XII (transmembrane tumour-associated isoforms), were investigated using a stopped-flow CO_2 hydrase assay.[33–38] Table 1 illustrates the enzyme inhibition constants (K_I) and the dose-response curves for determining the four CAs activity induced by the representative compounds **3c, 5b–d,** and **11a,b** presented in the Supplementary file, while Table 2 shows the estimated selectivity ratios (SRs). Acetazolamide (AAZ), a clinically used sulphonamide CAI, and SLC-0111 (Phase Ib/II clinical trials) were also used as control compounds in the tests. Based on the inhibitory results (as K_I values) listed in Table 1 for the synthesised analogues, the following structure–activity relationship (SAR) was estimated:

i. Sulphonamide analogues with K_I values ranging from 26.6 to more than 50 000 nM minimally inhibited the cytosolic isoform hCA I, showing that all synthetic compounds are weaker inhibitors than **AAZ** (K_I = 250 nM) except compounds **7b**, **9**, **13d,** and **15b** with K_I values of 156.3, 195.9, 92.6, and 26.6 nM, respectively. The most active analogue in this group, **15b**; K_I = 26.6 nM, has mercaptotriazole ring fused to the main scaffold triazine. The weakest inhibitors were **11a** and **11b;** K_I > 50 000 nM, which comprise substituted diphenyl pyrazoline ring.
ii. The target compounds showed K_I values ranging from 30.8 to 4585 nM, which showed lower activity than AAZ (K_I = 12.1 nM), according to analysis of the potency results for inhibiting hCA II. The investigated compounds exhibited better activity towards the hCA II than the hCA I isoform (**5d, 9, 13a,** and **15b** were the exemption). The presence of diphenyl pyrazole moiety was described the most active inhibitor towards hCA II **13d,** K_I = 30.8 nM, while analogue **9**, K_I = 4585 nM, was the weakest inhibitor.

Regarding SAR for Series **I**, the lipophilic moiety attached to hydrazone linker-controlled potency of inhibitors, where substituted pyrazole group enhanced the potency and reported the best inhibitory effect for analogue **7a,** K_I = 46.4 nM. Replacing pyrazole with isatin moiety reduced the potency as observed in analogue **3a,** K_I = 98.2 nM, while the existence of substituted phenyl group diminished the activity as perceived for compound **5a,** K_I = 175 nM. Concerning Series **II**, inclosing hydrazone linker within pyrazole ring **(13a–e)** exposed the strongest inhibitor **13d**, K_I = 30.8 nM. Fusing the triazole ring with the triazine scaffold **(15a,b)** diminished the potency as reported in **15b**, K_I = 46.2 nM. Meanwhile, partially saturated pyrazole moiety abolished activity of compounds **9** and **11a,b,** K_I = 4585, 4192, and 2131 nM, respectively.

(iii) With K_I values, the investigated compounds significantly suppressed the transmembrane tumour-associated isoform hCA IX

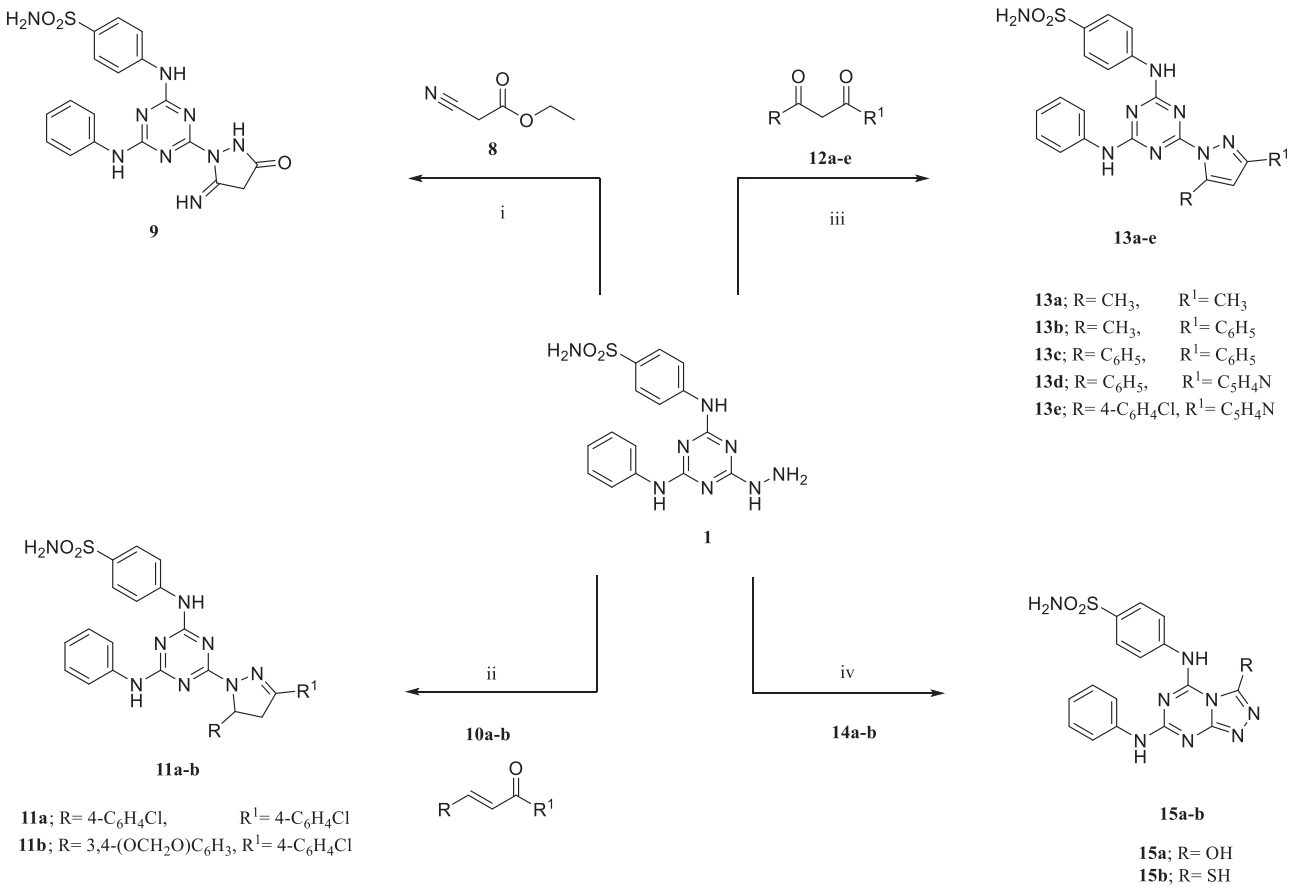

Scheme 2. Synthetic pathway of target sulphonamides **9, 11a,b, 13a–e,** and **15a,b.**

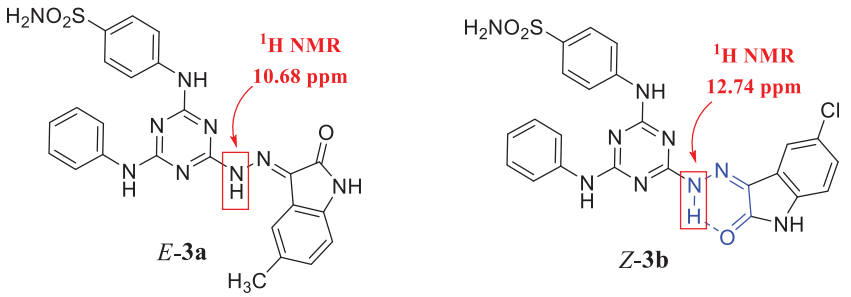

Figure 2. The *E*-isomer of compound **3a** and *Z*-isomer of compound **3b** with the pseudo-six-membered ring (in blue color).

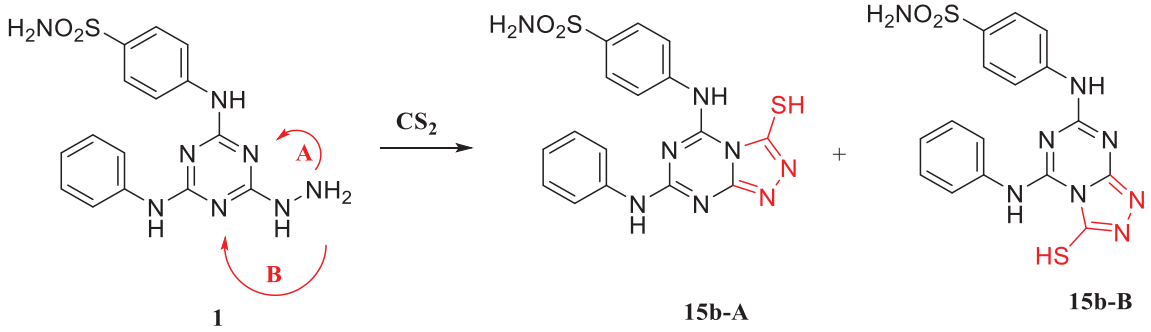

Scheme 3. The two proposed isomers of compound **15b** when refluxed with CS_2 in pyridine.

(28.6-871 nM). The diphenyl hydrazinyl methylidine analogue **5d** showed a stronger inhibitory effect with a K_I value (28.6 nM) comparable to **AAZ** (K_I = 25.8 nM). Meanwhile, comparing with SLC-0111 (K_I = 45 nM), compounds **3c**, **5b**, **5d**, **7b**, **11b,** and **15b** were more potent with K_I values of 43.8, 33.4, 28.6, 36.6, 31.9, and 40.7 nM, respectively. SAR study for Series **I** revealed that potency relied on lipophilic moieties attached to the hydrazone linker and decreased in the following order: phenyl derivatives

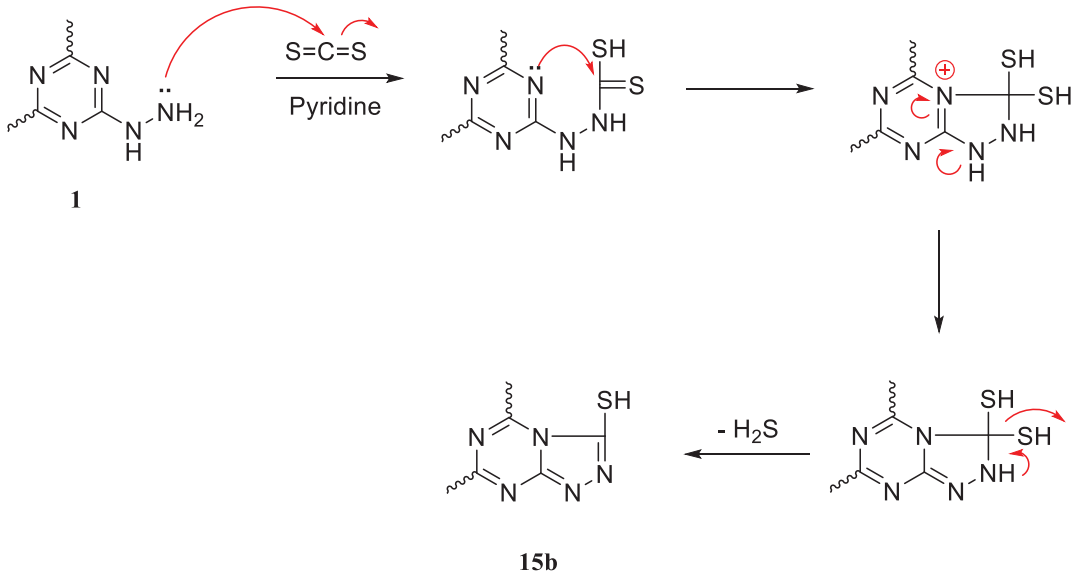

Scheme 4. A plausible mechanism for the formation of one of the two isomers regarding analogue **15b.**[31,32]

Table 1. Inhibition profile concerning human CA isoforms, off-target isoforms (hCA I and II), and the tumour-associated isoforms (hCA IX and XII) with triazine-based benzenesulfonamides 3a–c, 5a–d, 7a–e, 9, 11a,b, 13a–e, 15a,b, besides the standard inhibitors acetazolamide (AAZ) and SLC-0111 by a stopped-flow CO_2 hydrase assay.

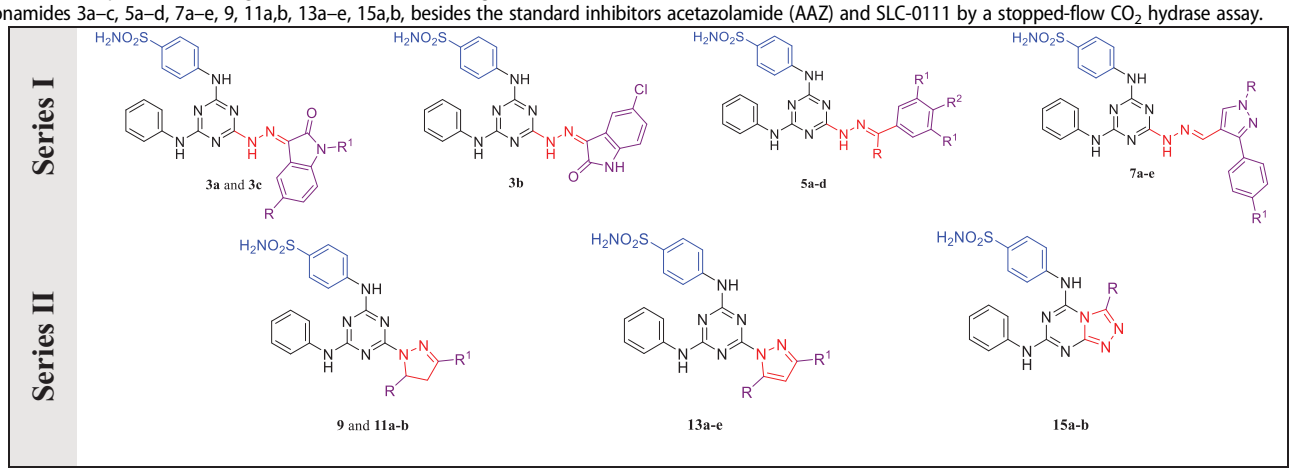

	K_I [a] (nM)			
Compounds	hCA I	hCA II	hCA IX	hCA XII
3a	8164	98.2	818.4	59.2
3b	8223	399.3	95.9	82.2
3c	3924	1516	43.8	24.4
5a	5111	175.4	575.5	64.1
5b	3523	668	33.4	14.9
5c	5309	2352	75.4	36.7
5d	4083	4291	28.6	31.3
7a	5811	46.4	68.6	85.5
7b	156.3	74.4	36.6	78.1
7c	8896	3147	47.3	439.0
7d	980.4	68.4	56.9	2185
7e	3720	2224	52.8	888.3
9	195.9	4585	443.0	27.3
11a	<50 000	4192	227	47.7
11b	<50 000	2131	31.9	8.29
13a	583.1	645.8	91.9	82.4
13b	368.9	114.3	94.7	77.8
13c	4710	2253	92.9	82.4
13d	92.6	30.8	91.8	89.9
13e	476.8	96.0	70.0	751.3
15a	728.0	704.7	871.4	40.6
15b	26.6	46.2	40.7	194.8
AAZ[b]	250.0	12.1	25.8	5.7
SLC-0111[b]	5080	960	45.0	4.5

[a]Mean from three different tests by a stopped-flow technique (approximately 5:10% of the reported numbers were erroneous).
[b]AAZ, a standard sulphonamide carbonic anhydrase inhibitor. SLC-0111is also provided for comparison.

(**5d**, K_I = 28.6 nM and **5b**, K_I = 33.4 nM) > pyrazole derivatives (**7b**, K_I = 36.6 nM) > isatin analogues (**3c**, K_I = 43.8 nM).

Regarding the isatin analogues **3a–c**, substitution of isatin with an electron-withdrawing group (chlorine atom) in **3b** and **3c** (K_I = 95.9 and 43.8 nM, respectively) potentiated the potency while an electron-donating group such as methyl group diminished the activity of analogue **3a** (K_I = 818.4 nM). In addition, N-alkylation of 5-chloroisatin with benzyl group **3c** (K_I = 43.8 nM) enhanced the activity more than the unsubstituted one, **3b** (K_I = 95.9 nM). The diphenyl pyrazole analogues, **7 b–e** (K_I ranging from 36.6 to 56.9 nM), showed better inhibition of hCA IX than one phenyl analogue **7a** (K_I = 68.6 nM). In the case of compounds **7c–e**, the substitution of phenyl ring at *para* position with either EWG or EDG reduced the inhibitory activity towards hCA IX than the unsubstituted analogue, **7b**.

Cyclic hydrazone linkers in five-membered rings reduced the potency of Series **II** compared to Series **I**. regarding SAR of Series **II**, potency declined in the following order: dihydropyrazoles (**11b**, K_I = 31.9 nM) > fused triazole derivatives (**15b**, K_I = 40.7 nM) ≫ pyrazole derivatives (**13e**, K_I = 70.0 nM). The fused triazol-3-ol analogue **15a** (K_I = 871.4 nM) was noted the least inhibitor in the series. Replacing the hydroxyl group in **15a** with the thiol group enhanced the inhibitory action against hCA IX by 21-fold, as noted in **15b** (K_I = 40.7 nM).

(iv) Despite being less active than **AAZ** (K_I = 5.7 nM), the target compounds significantly suppressed hCA XII. Their K_I values ranged from 8.29 to 2185 nM. Analogue **11b** with pyrazoline moiety directly attached to triazine scaffold exhibited the strongest inhibition of hCA XII with K_I = 8.29 nM. Concerning SAR of Series **I**, phenyl hydrazones (**5a–d**) exhibited the best activity as detected in **5b**, K_I = 14.9 nM. Exchanging the phenyl group with isatin reduced the potency of analogues **3a–c**, K_I = 59.2, 82.2, and 24.4 nM, respectively. Attaching phenylpyrazoles to the hydrazone linker (**7a–e**, K_{Is} from 78.1 to 2185.0 nM) diminished activity as observed in **7b**, K_I = 78.1 nM. Moreover, alkylation of isatin enhances the activity towards hCA XII as shown in compound **3c** (K_I = 24.4 nM) compared to compounds **3a** and **3b** with K_I = 59.2 and 82.2 nM, respectively. Target compounds in Series **II** (K_I = 8.29–751.3 nM) were better inhibitors for hCA XII than series **I** (K_I = 14.9–2185.0 nM). It was observed that SAR for Series **II** revealed that potency dropped in the following order: pyrazoline derivatives, **11b**, K_I = 8.29 nM ≫ fused triazoles, **15a**, K_I = 40.6 nM > pyrazoles, **13b**, K_I = 77.8 nM. In addition, replacing the hydroxyl group in **15a** (K_I = 40.6 nM) with thiol group diminished the inhibitory activity against hCA XII by about five times, as informed in **15b** (K_I = 194.8 nM). The dose-response curves for the determination of dissociation constants (K_I) for inhibition of hCA I, II, IX, and XII isoforms induced by representative compounds **3c, 5b–d,** and **11a,b** are illustrated in Figures S2–S7 (see Supporting information).

As a result, the diphenyl hydrazinyl analogue **5d** was the most effective anticancer substance. With K_Is of 28.6 and 31.3 nM for hCA IX and XII (the tumour-associated isoforms) and 4083 and 4291 nM for hCA I and II (the off-target isoforms), respectively, it showed the highest inhibitory impact relative to those isoforms.

Selectivity parameter. With high conservation in the all isoforms of CA active sites, the main sequence identity of the human CAs is at least 30%.[39] Designing isoform-selective CAIs for CA IX with few off-target actions has been difficult due to the high conservation of amino acid standing between hCA isoforms.[40] As demonstrated in Table 2, the compounds developed extraordinary selectivity towards hCA IX and XII (the tumour-associated isoforms) over the hCA I and II (off-target isoforms). The SRs, which are indicative parameters for enzyme selectivity and are pronounced in Table 2, were determined as the ratio between K_I for hCA I and II related to hCA IX and XII.

Table 2. Selectivity ratios for the inhibition of hCA IX and XII over hCA I and II for target compounds 3a–c, 5a–d, 7a–e, 9, 11a,b, 13a–e, 15a,b and the standard inhibitors acetazolamide (AAZ) and SLC-0111.

	Selectivity ratio (SR)[a,b] (K_I off-target CA/K_I target CA)			
Compounds	I/IX	II/IX	I/XII	II/XII
3a	9.97	0.12	137.91	1.66
3b	85.75	4.16	100.3	4.86
3c	89.59	34.61	160.82	62.13
5a	8.88	0.30	79.73	2.73
5b	105.48	20	236.44	44.83
5c	70.41	31.19	144.66	64.09
5d	142.76	150.03	130.44	137.09
7a	84.71	0.68	67.96	0.54
7b	4.27	2.03	2.00	0.95
7c	188.08	66.53	20.26	7.17
7d	17.23	1.20	0.45	0.03
7e	70.45	42.12	4.19	2.5
9	0.44	10.35	7.18	167.95
11a	220.26	18.47	1048.22	87.88
11b	1567.40	66.80	6031.36	257.06
13a	6.34	7.03	7.08	7.84
13b	3.89	1.21	4.7	1.47
13c	50.70	24.25	57.16	1.13
13d	1.01	0.34	1.03	0.34
13e	6.81	1.37	0.63	0.13
15a	0.84	0.81	17.93	17.36
15b	0.65	1.14	0.14	0.24
AAZ	10	0.48	43.86	2.10
SLC-0111	112.9	21.3	1128.9	213.3

[a]The K_I ratios indicate isozyme selectivity: A low-value ratio indicates the presence of a weak selective inhibitor.
[b]Selectivity as measured by the hCA I and II KI ratio in comparison to hCA IX and hCA XII.

i. The calculated SR I/IX were ranged from 1567.40 to 0.44 in terms of the selectivity towards hCA IX over hCA I. Twelve compounds exhibited SR (I/IX) (from 1567.40 to 17.23) higher than **AAZ** value (SR = 10) while four analogues displayed SR (I/IX) (from1567.40 to 142.76) higher than SLC-0111 value (SR = 112.9). Compound **11b** with pyrazoline linker carrying benzodioxole and phenyl rings showed extraordinarily great hCA IX selectivity, with SR (I/IX) = 1567.70 (156-times that of **AAZ**). Replacement of benzodioxole ring with *para*-chlorophenyl ring reduced selectivity of analogue **11a,** SR (I/IX) = 220.26. Compounds **5b**, **5d,** and **7c** revealed remarkable selectivity over **AAZ** with SR (I/IX) = 105.48, 142.76, and 188.08, respectively.
ii. The compounds demonstrated higher hCA IX selectivity over II, with SR (II/IX) ranged from 150.03 to 0.12 comparative to **AAZ** (SR = 0.48). The analogue **5d** with diphenyl hydrazone linker disclosed the highest hCA IX selectivity, with SR (II/IX) = 150.03 (312-times that of **AAZ**). Structural modifications to analogue **5d** *via* substitution with either EWG or EDG upon the phenyl ring diminished selectivity while further target compounds presented lower selectivity with SR (II/IX) between 66.80 and 0.12.
iii. The estimated SR (I/XII) for target molecules ranged from 6031.36 to 0.14 in terms of selectivity towards hCA XII over

hCA I. Eleven compounds showed SR (I/XII) (from 6031.36 to 57.16) higher than **AAZ** value (43.86). Fortunately, compound **11b** exhibited SR (I/XII) = 6031.36, about 6-times higher than SLC-0111 value with SR (I/XII) = 1128.9. Compounds **11a** and **11b** disclosed the best selectivity towards hCA XII, with SR (I/XII) = 1048.22 and 6031.36, which was 23 (1) and 137 (5) times that of **AAZ** (SLC-0111), respectively. The isatinylhydrazones, **3a–c** and phenylhydrazones, **5a–d,** reported high selectivity towards hCA XII, with SR (I/XII) ranging from 79.73 to 236.44. The selectivity was drastically reduced in **7a–e, 9, 13a–e,** and **15a,b,** having the pyrazole and triazole linkers.

iv. Thirteen analogues showed stronger selectivity for hCA XII than hCA II, with SR (II/XII) values ranging from 257.06 to 2.50 in comparison to AAZ, SR (II/XII) = 2.10. Compound **11b**, SR (II/XII) = 257.06 showed higher selectivity than SLC-0111, SR (II/XII) = 213.3. Compound **11b** with a pyrazoline linker exhibited the highest selectivity towards hCA XII, SR (II/XII) = 257.06, which was 122-times that of **AAZ** and higher than SLC-0111, SR (II/XII) = 213.3. Chemical modifications on the structure of compound **11b** dropped selectivity. Analogues **9,** SR (II/XII) = 167.95 and **5d,** SR (II/XII) = 137.09 showed high selectivity while analogue **7d,** SR (II/XII) = 0.03 reported the lowest selectivity.

Relying on the aforementioned findings, we have successfully developed new inhibitors with remarkable selectivity profiles towards hCAs IX and XII. Compound **11b** displayed excellent selectivity concerning hCAs IX and XII (the tumour isoforms) over hCAs I and II (the off-target) with SR values = 1567.40, 66.80, 6031.36, and 257.06. Additionally, it demonstrated relatively high effectiveness against hCAs IX and XII, with K_I values of 31.9 and 8.29 nM, respectively. The most effective analogue, **5d**, showed a respectable selectivity profile with SR values of 142.76, 150.03, 130.44, and 137.09 against hCA IX and XII, respectively.

In vitro evaluation of antiproliferative activity by NCI

In vitro *preliminary screening anticancer activity at 10 μM towards 60 cancer cell panels.* Series **I** (**3a–c**, **5a–d**, and **7a–e**) and Series **II** (**9**, **11a,b**, **13a–e**, and **15a,b**) of the newly synthesised triazine-based benzenesulfonamides underwent initial anticancer screening activity at the National Cancer Institute (NCI) as part of a screening effort in the United States. The NCI's preliminary *in vitro* 10 μM anticancer screening against the 60 cancer cell line panels representing nine types of cancer was carried out in accordance with the procedure using the novel analogues that were chosen and evaluated NCI. The treated cells' mean graph percent growth (G%) in comparison to the control cells that were not treated was used to represent the results for the test compound. This graph includes values for cytotoxicity (less than 0) and inhibition (cytostatic) (between 0 and 100). The results of tested compounds against sixty cancer cell lines were evaluated using the COMPARE tool. When tested at 10 μM, the anticancer activity of the compounds ranged from poor to excellent, with a wide range of cytotoxic activity against several cancer cell lines.[14] For target compounds, inhibition of percentage growth (GI%) was estimated as (100 – G%) and given in Table 3. Compounds **3b**, **3c, 5a, 7a, 7b, 7e, 9, 13a,** and **15a,b** that disclosed mean GI% less than 10% did not declare in Table 3. All one-dose and five-dose charts are presented in Supplementary files.

Inspection of biological data in Table 3 revealed that analogues of Series **II** were more potent (mean GI%, from 19 to 65) than target compounds of Series **I** (mean GI%, from 12 to 58), while

Table 3. Sixty human tumour cell lines *in vitro* subpanel at a concentration of 10 μM for the presence of compounds 3a, 5 b–d, 7c,d, 11a,b, and 13 b–e.

	Growth inhibition percentage (GI%)											
Subpanel cell lines	3a	5b	5c	5d	7c	7d	11a	11b	13b	13c	13d	13e
Leukaemia												
CCRF-CEM	73	56	89	72	51	43	85	63	45	89	62	–
HL-60(TB)	35	34	52	59	–	–	74	26	51	95	53	NT
K-562	56	33	85	66	41	28	67	32	48	88	43	NT
MOLT-4	57	59	118	81	89	68	82	51	55	95	64	NT
RPMI-8226	56	32	20	67	38	32	62	34	32	93	61	–
SR	66	38	112	80	67	51	94	59	31	99	44	NT
NSC lung cancer												
A549/ATCC	–	14	–	41	–	–	33	21	39	74	17	17
EKVX	–	18	13	44	22	15	43	21	30	59	21	15
HOP-62	11	–	73	–	–	–	24	–	–	36	17	–
HOP-92	44	–	104	24	–	–	25	16	10	73	52	–
NCI-H226	24	19	45	53	–	–	44	13	35	59	34	27
NCI-H23	31	25	72	49	14	–	45	–	–	76	21	16
NCI-H322M	26	–	62	–	–	–	35	15	–	42	26	36
NCI-H460	12	24	–	76	34	25	79	12	27	94	30	34
NCI-H522	42	–	50	22	–	–	16	12	29	41	18	41
Colon cancer												
COLO 205	17	23	11	39	–	–	91	29	17	90	12	22
HCC-2998	15	–	94	48	20	–	86	13	–	56	–	28
HCT-116	49	28	71	67	50	–	85	32	41	89	42	36
HCT-15	–	–	19	70	31	42	63	23	42	81	22	43
HT29	40	–	67	73	10	–	90	17	29	95	12	10
KM 12	27	18	38	64	40	34	94	40	27	90	26	43
SW-620	–	–	58	26	–	–	45	–	28	61	14	10
CNS cancer												
SF-268	32	13	78	40	24	18	40	17	30	62	23	20
SF-295	26	18	56	40	24	14	43	18	10	65	27	17
SF-539	14	15	125	35	11	17	41	18	19	62	25	20
SNB-19	15	10	85	26	20	13	38	13	19	49	18	10
SNB-75	–	–	74	35	–	13	32	–	–	43	17	31
U251	47	21	72	46	26	13	38	25	45	66	19	28
Melanoma												
LOX IMVI	53	NT	123	NT	33	18	87	27	27	NT	NT	32
MALME-3M	21	13	58	12	16	11	57	–	–	39	–	–
M14	NT	23	40	44	26	15	65	25	20	73	36	24
MDA-MB-435	29	33	43	50	28	16	60	23	30	73	28	14
SK-MEL-2	13	–	105	19	21	14	34	–	10	43	–	29
SK-MEL-28	20	20	65	24	19	13	52	23	18	45	17	–
SK-MEL-5	44	12	126	34	25	25	48	20	19	60	43	14
UACC-257	–	–	–	13	–	–	34	–	–	40	–	–
UACC-62	14	–	126	20	–	–	–	–	38	45	28	35
Ovarian cancer												
IGROV1	33	14	40	39	12	–	65	23	15	74	41	41
OVCAR-3	39	–	79	14	17	13	69	–	10	68	22	32
OVCAR-4	27	16	28	38	32	26	50	–	29	62	28	–
OVCAR-5	–	14	–	–	–	–	56	18	–	21	–	–
OVCAR-8	43	12	42	54	19	10	31	21	27	60	33	33
NCI/ADR-RES	–	–	–	34	–	–	37	–	–	55	–	13
SK-OV-3	–	–	–	11	–	–	35	–	–	34	–	–
Renal cancer												
786-0	23	21	74	46	23	15	34	15	16	79	40	21
A498	27	NT	–	NT	–	–	44	22	NT	NT	NT	22
ACHN	–	13	–	49	11	–	67	25	18	84	33	54
CAKI-1	33	25	–	50	–	–	57	13	27	79	43	65
RXF 393	27	42	45	74	31	30	103	39	29	77	41	36
SN 12 C	34	–	53	28	12	–	59	19	19	58	25	44
TK-10	–	–	–	–	–	–	10	–	–	–	–	19
UO-31	–	27	14	36	22	21	51	29	19	70	33	42
Prostate cancer												
PC-3	29	34	42	76	51	45	57	39	48	73	46	30
DU-145	24	15	49	32	12	–	49	11	25	67	25	24
Breast cancer												
MCF7	51	56	62	82	66	51	87	53	48	93	60	27
MDA-MB-231	12	13	101	28	–	–	45	26	23	62	41	32
HS 578 T	–	–	108	23	–	–	21	–	13	35	–	23
BT-549	19	–	114	32	12	–	26	–	17	47	31	37
T-47D	53	26	74	54	32	27	48	33	56	63	29	15
MDA-MB-468	45	22	157	29	19	14	73	22	30	88	42	29
GI% Mean	25	16	58	41	17	12	53	19	23	65	27	22

NT: not tested. "–" indicates GI% less than 10. GI% up to 60 indicates moderate activity, GI% up to 100 indicates strong activity, and GI% exceeds 100 shows lethal activity.

compounds in Series **I** displayed better selectivity than Series **II**. Regarding Series **I**, analogues **3a–c**, the presence of methyl group at phenyl ring of isatin moiety enhanced the activity of **3a**, mean GI% = 25 while exchanging methyl group with chloride atom abolished the anticancer activity for analogues **3b** and **3c**. The anticancer activity of phenylhydrazones, **5a–d**, was strongly potentiated upon the addition of two bromide atoms at the *meta* positions of the phenyl ring of analogue **5c.** Moreover, adding another phenyl ring to the hydrazone linker in **5d,** mean GI% = 41enhanced the cytotoxic activity. Concerning phenyl pyrazole analogues **7a–e**, analogues **7c** (mean GI% = 17) and **7d** (mean GI% = 12) with *para* chlorophenyl or *para* bromophenyl rings, respectively, showed better cytotoxic activity than unsubstituted phenyl analogue, **7b** or *para* methoxy substituted one, **7e** (both reported mean GI% less than 10).

The most active analogue **5c**, GI% = 58, demonstrated very strong activity (lethal effect) and selectivity against two leukaemia cell lines (MOLT-4, GI% = 118 and SR, GI% = 112), one of lung cancer cell lines (HOP-92, GI% = 104), one of CNS cancer cell lines (SF-539, GI% = 125), four of melanoma cell lines (GI% from 105 to 126), and four of breast cancer cell lines (GI% from 101 to 157). Analogue **5d,** mean GI% = 41, disclosed selective and strong cytotoxic effect against five leukaemia cell lines (GI% from 66 to 81), one of lung cancer cell lines (GI% = 76), four of colon cancer cell lines (GI% from 64 to 73), one of renal cancer cell lines (GI% = 74), one of prostate cancer cell lines (GI% = 76), and one of breast cancer cell lines (GI% = 82). Analogue **3a**, mean GI% = 25, reported strong and selective cytotoxicity towards two leukaemia cell lines only (GI% = 73 and 66). Compound **7c**, mean GI% = 17, selectively exhibited strong anticancer effect against two leukaemia cell lines (GI% = 89 and 67) and breast cancer, MCF7 cell line (GI% = 66). Finally, **7d**, mean GI% = 12, reported selective and strong cytotoxicity towards leukaemia, MOLT-4 cell line, GI% = 68.

Regarding Series **II**, the most active pyrazoline analogue **11a** with two *para* chlorophenyl rings (mean GI% = 53) reported broad and strong cytotoxic activity towards all leukaemia cell lines, non-small cell lung cancer; NCI-H460, all colon cancer cell lines except SW-620, melanoma cell lines; LOX IMVI, M14, and MDA-MB-435, ovarian cancer; IGROV1 and OVCAR-3, renal cancer; ACHN, and breast cancer cell lines; MCF7 and MDA-MB-468 (Table 3) whereas it displayed lethal effect (GI% = 103) against renal cancer cell line; RXF 393. Replacement of one *para* chlorophenyl ring in compound **11a** with a 1,3-benzodioxol ring of **11b** (mean GI% = 19) diminished the antiproliferative activity while it showed selective and strong cytotoxic activity towards leukaemia (CCRF-CEM) cell line (GI% = 63). Considering pyrazole derivatives **13a–e**, the most active analogue **13c** (mean GI% = 67) with diphenyl pyrazole scaffold displayed broad and strong anticancer activity towards almost all tested cancer cell lines. Replacement of one phenyl ring of **13c** with a pyridine ring reduced the cytotoxic activity of **13d** (mean GI% = 27) and **13e** (mean GI% = 22), while methyl phenyl analogue **13b** (mean GI% = 23) showed lower activity as well. Analogue **13d** revealed a selective and strong anticancer effect against three leukaemia cell lines (GI% from 64 to 61) and breast cancer, MCF7, cells (GI% = 60). Compound **13e** disclosed strong selective anticancer activity towards renal cancer, CAKI-1, cells (GI% = 65).

In vitro *anticancer screening at five doses towards 60 cancer cell panels.* Because they met the NCI's established threshold inhibition criteria, two compounds, **5c** (NSC 834606) and **13c** (NSC 832458), were screened and tested against the 60 cancer cell lines at 10-fold dilutions and five different concentrations (0.01, 0.1, 1,

Table 4. Five doses of *in vitro* anticancer activity results [a]against all sixty cancer cell lines expressed as GI_{50}[b] (μM), TGI[c] (μM), and LC_{50}[d] (μM) for compounds **5c** and **13c**.

	5c			13c		
Subpanel/cell lines	GI_{50}	TGI	LC_{50}	GI_{50}	TGI	LC_{50}
Leukaemia						
CCRF-CEM	11.1	41.6	>100	2.94	>100	>100
HL-60(TB)	22.0	60.9	>100	2.24	8.26	>100
K-562	23.4	>100	>100	2.62	10.8	>100
MOLT-4	19.7	52.3	>100	1.51	6.47	>100
RPMI-8226	22.8	93.5	>100	2.49	8.69	>100
SR	15.9	>100	>100	1.94	5.94	91.4
NSC lung cancer						
A549/ATCC	21.8	67.5	>100	3.18	17.9	>100
EKVX	21.4	69.2	>100	2.96	17.4	>100
HOP-62	21.3	58.9	>100	3.29	12.4	47.1
HOP-92	26.7	81.2	>100	2.16	6.18	41.1
NCI-H226	26.5	98.2	>100	2.52	11.0	>100
NCI-H23	20.9	50.1	>100	2.84	9.12	30.5
NCI-H322M	14.2	27.3	52.4	2.78	29.9	>100
NCI-H460	19.6	60.1	>100	2.07	4.66	11.7
NCI-H522	16.8	42.4	>100	2.29	7.39	>100
Colon cancer						
COLO 205	16.0	29.8	55.5	1.78	3.27	6.01
HCC-2998	14.8	29.2	57.8	2.98	6.84	33.4
HCT-116	17.7	38.9	85.5	1.74	3.39	6.58
HCT-15	32.3	>100	>100	3.08	11.2	>100
HT29	19.6	49.1	>100	2.38	5.48	16.5
KM 12	17.5	37.1	78.9	2.77	8.20	>100
SW-620	17.2	42.4	>100	3.52	32.1	>100
CNS cancer						
SF-268	19.9	58.6	>100	3.97	>100	>100
SF-295	22.2	60.2	>100	3.02	10.5	>100
SF-539	17.9	41.3	95.0	2.66	10.3	44.5
SNB-19	14.2	27.7	53.9	3.44	20.9	>100
SNB-75	18.6	61.7	>100	4.61	>100	>100
U251	20.0	71.0	>100	2.91	10.3	39.6
Melanoma						
LOX IMVI	15.8	30.4	58.6	NT	NT	NT
MALME-3M	14.7	34.8	82.0	2.43	7.09	45.2
M14	18.8	45.7	>100	3.22	12.5	55.7
MDA-MB-435	17.8	40.6	93.0	3.32	12.9	>100
SK-MEL-2	15.7	38.1	92.3	2.39	6.95	30.1
SK-MEL-28	18.1	40.6	91.2	3.87	16.9	>100
SK-MEL-5	14.9	28.6	54.8	2.33	5.54	17.8
UACC-257	20.6	47.9	>100	3.26	23.3	>100
UACC-62	14.5	28.3	55.3	1.81	3.76	7.80
Ovarian cancer						
IGROV1	18.5	42.2	96.4	2.72	11.4	81.5
OVCAR-3	21.4	63.1	>100	2.24	4.97	19.2
OVCAR-4	23.2	81.4	>100	2.77	9.32	>100
OVCAR-5	22.7	62.6	>100	3.34	14.3	72.7
OVCAR-8	26.9	>100	>100	3.22	16.0	>100
NCI/ADR-RES	>100	>100	>100	2.93	11.0	65.5
SK-OV-3	21.3	61.9	>100	5.37	>100	>100
Renal cancer						
786-0	15.1	44.3	>100	3.09	10.6	76.4
A498	13.3	36.6	>100	3.33	8.08	27.0
ACHN	24.8	93.8	>100	2.59	9.95	88.5
CAKI-1	24.0	85.7	>100	2.45	9.55	>100
RXF 393	14.7	32.8	73.3	1.99	5.23	22.8
SN 12 C	15.6	32.1	66.0	1.47	2.88	5.63
TK-10	27.7	87.0	>100	3.87	8.93	>100
UO-31	26.7	>100	>100	2.38	10.0	49.4
Prostate cancer						
PC-3	19.5	55.2	>100	2.37	7.89	>100
DU-145	16.1	30.2	56.5	3.16	13.0	>100
Breast cancer						
MCF7	16.9	45.4	>100	2.27	6.61	51.6
MDA-MB-231	17.2	47.4	>100	1.81	3.85	8.18
HS 578 T	77.6	81.3	>100	4.31	62.7	>100
BT-549	16.8	42.7	>100	2.24	5.54	26.7
T-47D	7.39	27.3	85.6	2.96	13.2	>100
MDA-MB-468	2.94	15.5	>100	2.31	6.95	92.3

[a]*In vitro* human cancer cell lines screen data from NCI. [b]Molar concentration necessary to inhibit 50% of growth of cancer cell line. [c]Molar concentration necessary to inhibit 100% of growth of cancer cell line. [d]Molar concentration necessary to kill 50% of cancer cell line.
NT: not tested.

10, and 100 M).[14] Following the described experimental techniques, the SRB (sulforhodamine-B) protein assay was used to compare the viability of treated *versus* untreated cells.[41]

The results of this assay are stated in GI_{50} (molar concentration required to inhibit 50% of the growth of cancer cell line), TGI (molar concentration required to inhibit 100% of the growth of cancer cell line), and LC_{50} (molar concentration required to kill 50% of cancer cell line) after a 48-h incubation period for each cell line tested.[42,43] Table 4 lists the estimated GI_{50}, TGI, and LC_{50} values for all 60 cancer cell lines for these two compounds for each of the nine cancer types. With the best GI_{50} = 1.47 μM, TGI = 2.88 μM, and LC_{50} = 5.63 μM against the 60-NCI cancer cell lines, the tested compounds (**5c** and **13c**) showed outstanding action against cancer cells, according to the findings of anticancer screening of the five-dose.

Compound **5c** displayed strong cytotoxic activity with GI_{50} values ranging from 2.94 to 32.2 μM (except against HS578T (77.6 μM) and NCI/ADR-RES (>100 μM)), TGI values ranging from 15.5 to >100 μM, and LC_{50} values ranging from 52.4 to more than 100 μM. Compound **5c** demonstrated the greatest cytotoxic activity towards NCI-H322M NSC lung cancer cell line, LC_{50} = 52.4 μM, while it exposed the best cytostatic activity towards MDA-MB-468 breast cancer cell line with GI_{50} = 2.94 μM and TGI = 15.5 μM followed by its effect on T-47D on same cancer with GI_{50} = 7.39 μM and TGI = 27.3 μM as displayed in Table 4.

Compound **13c** reported stronger cytotoxic activity than **5c**, with GI_{50} values ranging from 1.47 to 5.37 μM (all in the single-digit micromolar range), TGI values ranging from 2.88 to >100 μM, and LC_{50} values ranging from 5.63 to more than 100 μM. It revealed the greatest cytostatic activity towards the majority of the cancerous cell lines, including; MOLT-4 "most affected one in leukaemia" with GI_{50}= 1.51 μM, NCI-H460 "most affected one in lung cancer" with GI_{50}= 2.07 μM, HCT-116 "most affected one in colon cancer" with GI_{50}= 1.74 μM, SF-539 "most affected one in CNS cancer" with GI_{50}= 2.66 μM, UACC-62 "most affected one in melanoma" with GI_{50}= 1.81 μM, OVCAR-3 "most affected one in ovarian cancer" with GI_{50}= 2.24 μM, SN 12 C "most affected one in renal cancer" with GI_{50} = 1.47 μM, PC-3 "most affected one in prostate cancer" with GI_{50}= 2.37 μM, and MDA-MB-231 "most affected one in breast cancer" with GI_{50}= 1.81 μM. It exhibited the best cytotoxic action towards the SN 12 C renal cancer cell lines with LC_{50}= 5.63 μM (Table 4).

A mean graph midpoints (MG-MID) were computed, resulting in averaged activity parameters across all cell lines. The GI_{50}-MID values for the compounds **5c**, **13c**, and **5-FU** were 189.01, 25.08, and 65.16 μM, respectively (Table 5 and Figure 3). The ratios were calculated by dividing the full panel MID by their individual subpanel MID and were used to determine the selectivity of these compounds (the sensitivity average of the whole cell lines of a particular subpanel). SRs between 3 and 6 indicate moderate selectivity, whereas ratios of more than 6 reveal the best selectivity towards the associated cell line. The compounds that match none of these requirements are classed as non-selective.[44,45] Accordingly, the studied compounds, **5c** and **13c** are non-selective

Table 6. Cytotoxic activities of compounds **5d** and **13c** against MCF7 (breast cancer), and NCI-H460 (lung cancer) under hypoxia compared to 5-FU.

	IC_{50} ± *SD* (μM)[a]	
Compound No.	MCF7 (Breast cancer)	NCI-H460 (Lung cancer)
5d	15.02 ± 0.02	10.12 ± 0.03
13c	3.03 ± 0.01	4.62 ± 0.02
5-FU	4.10 ± 0.02	6.77 ± 0.02

[a]IC_{50} values are the mean ± *SD* of three experiments.

Table 5. Selectivity ratios of the analouges **5c** and **13c** in comparison to **5-FU** towards nine tumours.

	5c			13c			5-FU		
Panel	MID[a]	MID[b]	Selectivity[c]	MID[a]	MID[b]	Selectivity[c]	MID[a]	MID[b]	Selectivity[c]
Leukaemia	19.15	21.06	1.09	2.29	2.78	1.21	3.24	7.24	2.23
NSC lung cancer	21.02		1.00	2.67		1.04	20.11		0.36
Colon cancer	19.30		1.09	2.60		1.06	1.83		3.95
CNS cancer	18.80		1.12	3.43		0.81	17.02		0.42
Melanoma	16.76		1.25	2.82		0.98	7.92		0.91
Ovarian cancer	33.42		0.63	3.22		0.86	5.77		1.25
Renal cancer	20.23		1.04	2.64		1.05	0.88		8.22
Prostate cancer	17.80		1.18	2.76		1.00	1.36		5.32
Breast cancer	23.13		0.91	2.65		1.04	7.03		1.02
GI_{50}-MID	189.01			25.08			65.16		

MID[a]: Average sensitivity of all cell lines of a particular subpanel in μM; MID[b]: Average sensitivity of all cell lines (μM); Selectivity[c]: ratio MID[a]: MID[b].

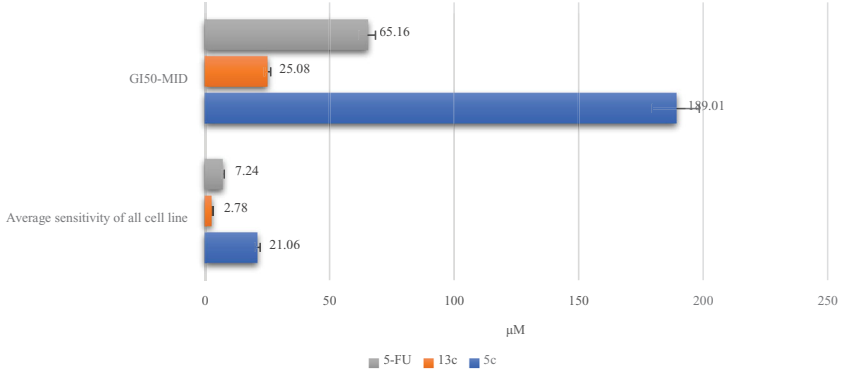

Figure 3. GI_{50}-MID and average sensitivity of all cell lines (μM) of **5c** (blue), and **13c** (orange), in comparison to **5-FU** (grey).

and have a broad-spectrum antitumor effect against the examined nine tumour subpanels, with SRs ranging from 0.63 to 1.25.

Compound **13c** showed the best potency with average MID = 2.78 μM, which was better than **5-FU**, average MID = 7.24 μM, and **5c**, average MID = 21.06 μM. It disclosed the greatest potency and selectivity towards leukaemia, MID = 2.29 μM, with selectivity = 1.21, while it demonstrated better potency and selectivity towards NSC lung cancer, MID = 2.67 μM, selectivity = 1.04 compared to **5c,** MID = 21.02 μM, selectivity = 1.00 and **5-FU,** MID = 20.11 μM, selectivity = 0.36. Compound **5c** with average MID = 21.06 μM, showed the greatest potency and selectivity against melanoma, MID = 16.76 μM, selectivity = 1.25 which were more selective than **13c,** selectivity = 0.98 and **5-FU,** selectivity = 0.91 (Table 5 and Figure 3).

Activities of compounds 5d and 13c against MCF7 and NCI-H460 cancer cell lines under hypoxia

Using the SRB assay in hypoxic circumstances (1% O_2, 5% CO_2) at 37 °C, sulphonamide derivatives **5d** and **13c** were tested for their *in vitro* cytotoxic effects against the MCF7 (breast cancer) and NCI-H460 (lung cancer) cell lines.[46] 5-FU was applied as a positive control, and the concentration needed to inhibit cell viability by 50%, or IC_{50}, was determined (Table 6). Compound **13c** displayed the most potent activity towards MCF7, and NCI-H460, with IC_{50} values of 3.03 ± 0.01 μM (by five-folds) and 4.62 ± 0.02 μM (by 2-fold), respectively, compared to compound **5d**, which showed IC_{50} values of 15.02 ± 0.02 and 10.12 ± 0.03 μM, respectively. Additionally, compound **13c** has superior activity against MCF7 and NCI-H460 compared with positive reference drug (5-FU) with IC_{50} values of 4.10 ± 0.02 μM and 6.77 ± 0.02, respectively.

Table 7. Anti-proliferative activity of compound **13c** and **5-FU** against normal human cells.

	IC_{50} ± *SD* (μM)[a]	
Compound No.	LO2	HK2
13c	30.88 ± 0.98	53.39 ± 1.58
5-FU	18.71 ± 0.48	34.01 ± 0.98

[a]IC_{50} values are the mean ± *SD* of three experiments.

Toxicity of 13c and 5-FU towards normal human cells

13c demonstrated a strong tumour proliferation suppression effect *in vitro* as a possible anticancer cancer agent. We investigated **13c**'s possible toxicity towards healthy human cells to learn more about its therapeutic properties. For this, LO2 (human normal liver cells) and HK2 (human kidney proximal convoluted tubule epithelial cells), two different types of nontumorigenic cell lines, were used.[47] The results reported in Table 7 indicated that **13c** exhibited a far safer impact on normal human cells (LO2 and HK2) with IC_{50} values of 30.88 ± 0.98 and 53.39 ± 1.58 μM, respectively, using 5-FU as a positive control, which presented IC_{50} values of 18.71 ± 0.48 and 34.01 ± 0.98 μM, respectively.

Compound 13c suppresses the migratory of NCI-H460 cells

The ability of **13c** to prevent the metastasis of NSCLC cells *in vitro* was examined because tumour cell migration is one of the key factors contributing to the death of cancer patients.[48] The effect of **13c** on NSCLC cell migration was examined using transwell invasion assays and wound healing experiments. In contrast to cells treated with a vehicle, compound **13c** greatly reduced the migration of NCI-H460 cells, as seen in Figure 4. This suggests that **13c** may be a potential choice for preventing metastasis.

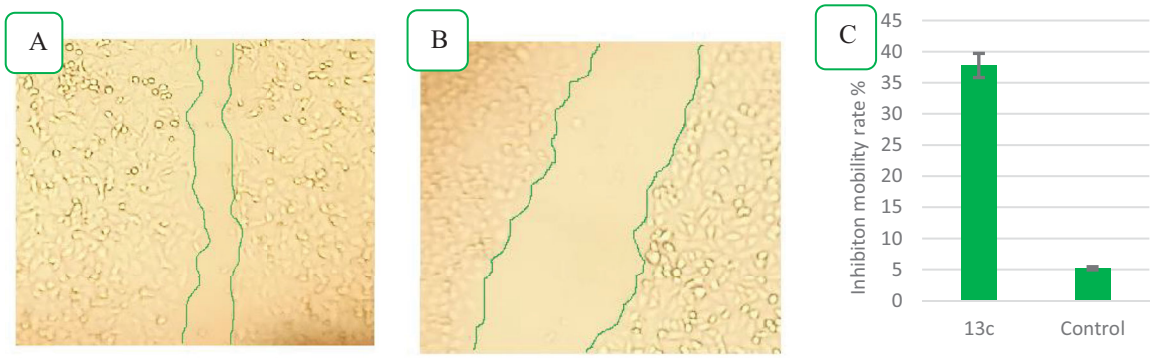

Figure 4. Compound **13c** reduces the migratory capacities of NCI-H460 cells *versus* control. (A) Effect of negative control on wound healing, (B) Effect of compound **13c** on wound healing, and (C) Quantitative analysis of the percentage of mobility inhibition rate. The values are the mean ± SD of three experiments.

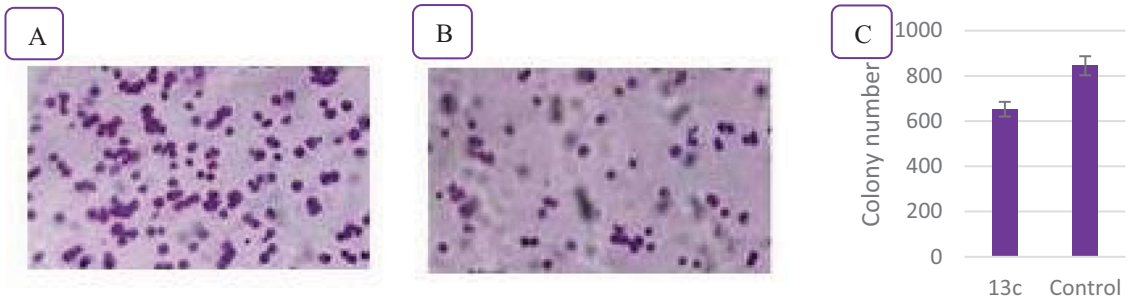

Figure 5. The influence of compound **13c** on the clonogenicity of NCI-H460. (A) Effect of negative control on clonogenicity of NCI-H460 cells, (B) Effect of compound **13c** on clonogenicity of NCI-H460 cells, and (C) Quantitative analysis of the colony number. The values are the mean ± SD of three experiments.

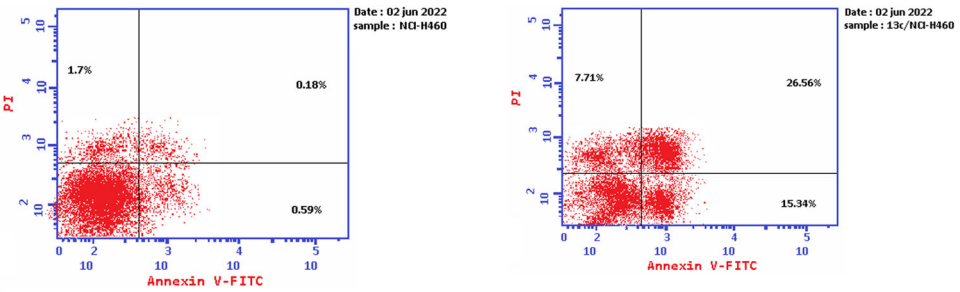

Figure 6. Effect of compound **13c** (right panel) and DMSO (left panel) on the proportion of annexin V-FITC-positive staining in NCI-H460 cells during an apoptosis experiment. The four quarters were designated as LL for viable, LR for early apoptosis, UR for late apoptosis, and UL for necrotic.

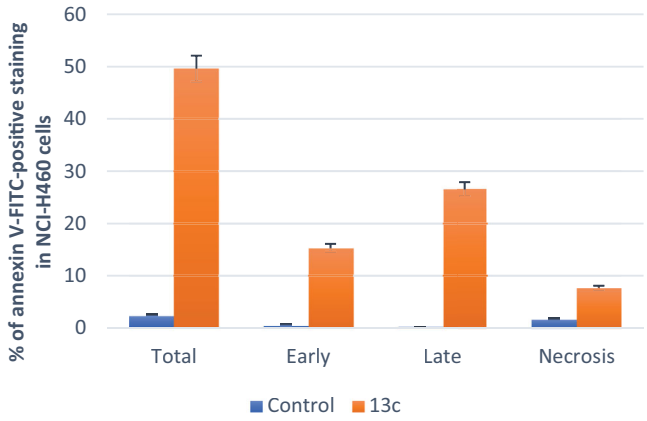

Figure 7. The percentage of NCI-H460 cells stained positively for annexin V-FITC in the apoptosis assay is affected by compound **13c** and DMSO. The values are the mean ± SD of three experiments.

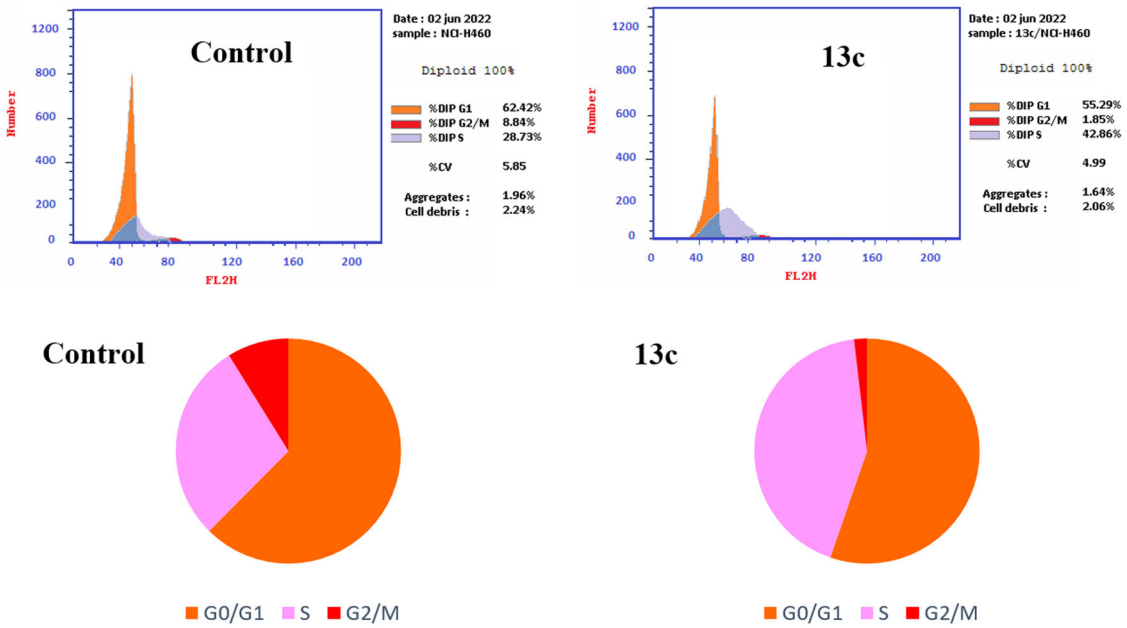

Figure 8. Cell cycle analysis of compound **13c** (left panel) and DMSO (right panel)-treated NCI-H460 cells (right panel).

Colony formation assay in NSC lung cancer, NCI-H460 cells

The colony-forming assay, an *in vitro* test for cell survival, assesses a cell's capacity to multiply into a colony. Each cell in the population is tested to see if it divides widely and forms foci. Additionally, it keeps track of the cells that have kept their ability to form colonies after being exposed to agents that cause cell death (chemotherapeutic agents or radiations).[49] Compound **13c**'s effective and broad-spectrum proliferative inhibition in this work motivated us to investigate how it affected NCI-H460 cells' ability to form cell colonies (one of the most sensitive cell lines as determined in previous NCI assays). Ten days following the compound **13c** treatment, colony development was assessed. Compound **13c**

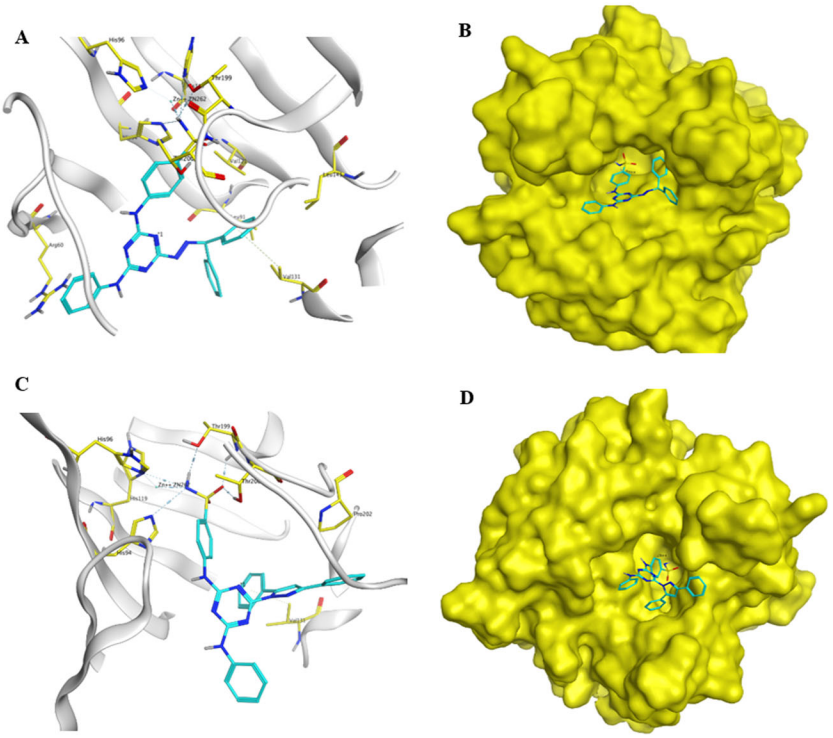

Figure 9. Docking of compounds **5d** and **13c** within the active site of hCA IX (PDB, ID: 3IAI). (A and C) The 3D binding mode of compounds **5d** and **13c** with hCA IX. The analogues **5d** and **13c** are coloured in cyan. The surrounding residues in the binding pocket are coloured in yellow. The hydrogen bond is depicted as a magenta dashed line. (B and D) The surface binding mode of hCA IX with compounds **5d** and **13c** viewing large cavity size in the active site filled with two bulky phenyl rings attached to hydrazone linker in **5d** and pyrazole linker in **13c**.

Table 8. Outcomes for docking of target compounds, **5d** and **13c** in the hCA IX active site (PDB, ID: 3IAI).

Compound	Docking Score (kcal/mol)	Ionic interaction	H-bond interaction	Hydrophobic interaction
5d	−9.97	Zn^{2+}	Thr199 and Thr200	Arg60, Leu91, His94, His96, His119, Val121, Val131, Leu141.
13c	−8.92	Zn^{2+}	Thr199 and Thr200	His94, Val131, Pro202

was able to significantly reduce colony formation in the tested cells when compared to the untreated control, as shown in Figure 5.

Annexin V–FITC apoptosis assay

The primary method by which drugs kill cancer cells is by the activation of apoptosis.[50,51] Cellular alterations brought on by apoptosis include translocating phosphatidylserine (PS) from the inside to the outside *via* the plasma membrane. PS can bind to Annexin-V, making it sensitive to PS on the plasma membrane's outer side.[52,53] We used cytometric assay to separate the apoptosis from the necrosis mechanism of NCI-H460 (melanoma) cells death caused by the most potent analouge, **13c**. NCI-H460 cells were stained with AV/PI for 24 h using compound **13c** (10 μM). Results from treating NCI-H460 cells with compound **13c** for 24 h are displayed in Figures 6 and 7. We find that the early apoptosis ratio increased from 0.59% in the negative control (DMSO) to 15.34% (Figure 6, lower-right quarter of the cytogram) and that the late apoptosis ratio increased significantly from 0.18 to 26.56%. These data demonstrate that the necrotic pathway is not the mechanism driving compound **13c**-induced programmed cell death but rather the apoptotic pathway.

In vitro cell cycle analysis

Antitumor drugs can cause S-phase cell cycle arrest and apoptosis *via* activating signalling pathways.[54–58] The proliferation of cells in various cell cycle phases (pre-G1, G1, S, and G2/M) is measured by flow cytometry.[59] The NCI-H460 cell line was used to further examine the effects of the most active compound, **13c**, on cell cycle progression (Figure 8). As a negative control, we employed the solvent DMSO. In a nutshell, we gave NCI-H460 cells 24 h of exposure to 10 μM of compound **13c**. Compound **13c** disrupted the NCI-H460 cells' typical cell cycle. An increase in cells in the S phase (42.86%) in comparison to the control suggested that there was a considerable impact on the proportion of apoptotic cells (28.73%). Cell cycle arrest resulted from a considerable drop in the proportion of cells in the G0/G1 and G2/M phases (55.29% and 1.85%, respectively) as compared to the control (62.42% and 8.84%, respectively). The alteration of the S-phase arrest is a crucial observation for compound **13c** to induce apoptosis in NCI-H460 cells (Figure 8).

In silico analysis

Molecular docking analysis

In hCA IX, having the active site at the bottom side of the conical cavity, the three residues of histidine (His 94, 96, and 119) make the coordination interaction with the zinc ion at the bottom of the active site.[60,61] The target compounds demonstrated potential for being potent and selective hCA IX inhibitors. Consequently, the mechanism of action of target compounds were explored *via* evaluating the docking profiles and amino acid interactions for

Table 9. Calculated binding free energy of the compound **5d** (kJ/mol).

Complex **5d**-hCA IX; $\Delta G = -118.76 \pm 30.58$			
Van der Waal energy	-154.67 ± 17.16	Polar solvation energy	192.19 ± 25.08
Electrostatic energy	-133.32 ± 27.50	SASA energy	-22.96 ± 1.55

analogues, **5d,** and **13c** within the active region of hCA IX (PDB, ID: 3IAI). The docking process was achieved by MOE program.[33,62] The docking of compounds **5d** and **13c** on the hCA IX active site illustrated proper fitting and good energy scores (S), suggesting the inhibitory activity of these sulphonamides as displayed in Figure 9 and Table 8. The docking scores (S) and interactions of inhibitors **5d** and **13c** with various amino acids on the active site of hCA IX were reported in Table 8. The deprotonated sulphonamide group's nitrogen and the triple histidines were coordinated to the Zn^{2+} atom conferring to molecular docking of compound **5d** (Figure 9). The gatekeeper amino acids of this enzyme, Thr199, and Thr200, were joined by two H-bonds and one H-bond, respectively, to the sulphonamide groups of docked inhibitors.[63] Furthermore, the hydrophobic region of the hCA active site (Leu91, Val121, Val131, and Leu141) was attracted to the two phenyl rings that were linked to the methylidene hydrazone moiety. The hydrophobic interaction between the N-phenyl segment and Arg60 was observed (Figure 9(A,B)). In **13c**, the nitrogen atom of sulphonamide showed coordination interaction with the Zn^{2+} atom and could form H-bonds with Thr199 and Thr200. Val131 and Pro202 of the CA active site's hydrophobic region revealed an interaction with the diphenylpyrazole moiety of **13c** hydrophobically (Figure 9(C,D)).

Molecular dynamics (MD) simulation

The MD simulation using the GROMACS program[64–66] was performed to study the behaviour of the most potent compound **5d** within the target hCA IX through the time of the simulation (100 ns) under comparable physiological conditions.

Analysis of the root mean square deviation (RMSD). Quantitatively to measure the degree of divergence of complex protein structure with ligand from its initial behaviour, the root mean square deviation (RMSD) was explored.[67] The RMSD aids in assessing the system's stability during the simulation. For this, a control system (a ligand-free structure) and complex were set up in two separate MD simulations. A 100-ns MD simulation was used to examine the stability and convergence of compound **5d** in its complex with hCA IX where the backbone atoms' RMSD value was calculated as illustrated in Figure S8. The results suggested that complex-maintained equilibrium throughout the simulation time. The apoprotein and the compound **5d**-bound complex's RMSD values ranged from 0.17 to 0.33 nm. Over the duration of the simulation, compound **5d** displayed consistent behaviours inside the receptor pocket and moved further into the binding pocket. This could account for the strong inhibitory activity of **5d** against hCA IX.

Analysis of the root mean square fluctuation (RMSF). The root mean square fluctuation (RMSF) was studied to represent the local changes that occur within the protein structure due to the presence of the recommended inhibitor.[68] It revealed the flexibility degree of the protein throughout the simulation time. The most fluctuation was observed within the $0.03 - 0.23$ nm range. In general, the native unbound hCA IX was more flexible than the comparable residues in the compound **5d**-bound complex. The values of the key residues implicated in intermolecular interactions, such as Arg60, Leu91, His94, His96, His119, Val121, Val131, Leu141, Thr199, and Thr200, were also found to be at the bottom of the curve (0.03–0.09 nm) after the RMSF analysis. The docked molecules' stability at the binding site was aided by these low-fluctuating residues (supplemental Figure S9).

Analysis for the radius of gyration (R_g). The size and compactness of protein molecules are indicated by the radius of gyration (R_g). When ligands are bound, the R_g can be utilised to monitor the folding and unfolding of protein structures.[69] Generally, the R_g values for the drug-bound complexes were nearer to the native unbound hCA IX (Figure S10). The average R_g values for compound **5d** and hCA IX were measured to be 1.74–1.80 nm. A higher R_g denotes a less compact or more unfolded protein–ligand interaction. However, a protein is said to be securely folded if its R_g value stays constant during the MD simulation. If the value of R_g changes with time, it is seen as unfolded. As seen in Figure S10, each complex revealed extremely comparable characteristics in terms of compactness and practically consistent values of R_g when compared to the unbound protein.

Analysis of solvent-accessible surface area (SASA). The protein's solvent-accessible surface area (SASA) was investigated both in the absence and presence of ligands. The amount of conformational changes that the aqueous solvent can access is predicted with the help of the protein-ligand complex's SASA computation.[70] Therefore, throughout the 100-ns MD simulation, the SASA was employed to assess interactions between the complex and the solvent. Figure S11 displays the SASA *versus* simulation time curve for the unbound protein and protein-ligand complexes. The SASA averages for compound **5d** and CA ranged from 120 to 133 nm^2. The extended surface formed by a piece of the bound ligand surface sticking out from the protein surface upon compound **5d** binding triggered the SASA to rise slightly.

Analysis of hydrogen bond. Hydrogen bonds that developed between the receptor and ligand help to stabilise the protein-ligand complex. Additionally, it affects the specificity, metabolisation, and adsorption of drugs and their design.[71] Therefore, each ligand-protein complex's hydrogen bonds were examined. Following a 100-ns simulation, Figure S12 shows the total number of hydrogen bonds found in the complex. One to three hydrogen bonds were found in the hCA-**5d** complex, and one of them was constantly present throughout the simulation time. In addition, during the course of the simulation, compound **5d** revealed a consistent hydrogen-bonding pattern, as seen in Figure S12. We could infer from the above-described H-bond study that compound **5d** was tightly and successfully attached to the hCA IX. The CA-**5d** complex's hydrogen bonds contact frequency is disclosed in Figure S13.

Binding energy estimation by MM/PBSA method. The molecular mechanics/Poisson Boltzmann surface area (MM/PBSA) approach was chosen for rescoring complexes because it computes the free energy of binding more quickly than other force field-based

methods like the free energy perturbation (FEP) or thermodynamic integration (TI) methods.[69] The MM/PBSA calculation was performed using g_mmpbsa software. The calculated binding free energies are illustrated in Table 9. The van der Waals attraction, electrostatic interactions, and non-polar solvation energy were the key contributors to the binding, while the polar solvation free energy weakened the complexation, according to this study. The average overall binding free energy of the complex is − The va ± 30.583 kJ/mol.

Conclusion

With the use of the dual-tail method, we were able to develop potent and selective hCA IX inhibitors that could potentially act as cytotoxic agents. Twenty-two novel anticancer compounds were designed, synthesised, characterised, and biologically tested. With K_I values ranging from 26.6 to more than 50 000 nM (hCA I); 30.8–4585 nM (hCA II); 28.6–871 nM (hCA XI); and 8.29–2185 nM (hCA XII), all assayed hCA isoforms were inhibited by analogues to varying degrees. The majority of the target compounds displayed a strikingly better selectivity towards CA IX than AAZ. Superior to AAZ (K_I = 25.8 nM, SR (I/IX) = 10 and SR (II/IX) = 0.48), **5d** was shown to be the most active hCA IX inhibitor in this investigation with (K_I = 28.6 nM, SR (I/IX) = 142.76 and SR (II/IX) = 150.03), making it more potent and selective. However, in accordance with US-NCI policy, all target compounds were examined for their anticancer efficacy at 10^{-5} M towards 60 cancer cell lines. The strongest antiproliferative actions were demonstrated by analogues **13c** (mean GI% = 65) and **5c** (mean GI% = 58). Comprising hydrazone linker in a rigid cyclic structure such as pyrazole ring enhanced anticancer activity of analogue **13c** compared to flexible hydrazone linker in analogue **5c**. Bulky and lipophilic tails attached to either pyrazole linker in **13c** or hydrazone linker in **5c** enhanced anticancer activity due to the lipophilic nature and large cavity size of the hCA IX active site. Moreover, compound **13c** was screened for apoptosis and disturbance of cell cycle in NCI-H460 cells, where It was arrested at the S phase of the cell cycle, and the percent of annexin V-FITC positive apoptotic cells increased from 0.18 to 26.56%. Compound **13c** was markedly able to inhibit colony formation in NCI-H460 and suppressed the migratory of NCI-H460 cells compared to untreated control. In order to explain the obtained biological data, a molecular modelling investigation for selected analogues inside the hCA IX active sites was achieved.

Experimental protocols

Chemistry

Using a Stuart SMP30 apparatus, melting points were found in open-glass capillaries and were not adjusted. The Sigma-Aldrich, Alfa-Aesar, and Merck companies provided all of the organic chemicals and solvents, which were all employed without additional purification. Pre-coated aluminium sheets and silica gel (Silica 60 F_{254}, Supelco Co., Poole, UK) are frequently used in analytical thin-layer chromatography (TLC) to check reaction completion and verify the purity of the compounds utilising the developing system: *n*-hexane, ethyl acetate (2:3) eluent by using a UV light with a wavelength of 254 nm. The Faculty of Pharmacy and Science, Mansoura University, Mansoura, Egypt, performed ^{1}H NMR, ^{13}C NMR, and APT spectra using a Bruker or JEOL instrument at 400–500 MHz for ^{1}H NMR and at 100–125 MHz for ^{13}C NMR. TMS was used as an internal standard, and chemical shifts were recorded in ppm on the scale using DMSO-d_6 as the solvent. Compounds **3a** and **3b** were dissolved in a mixture of DMSO-d_6 and DMF. Values for the coupling constant (*J*) were calculated in Hertz (Hz). The following splitting patterns are identified: singlet (s), wide singlet (br. s), doublet (d), triplet (t), and multiplet (m). The extremely low solubility of some compounds was the cause of the absence of some signals in ^{13}C NMR spectra. Thermo Scientific's ISQ Single Quadruple MS was used to record the electron impact mass spectra. C, H, N, and S underwent microanalysis on a PerkinElmer 2400, and the results were within ±0.4% of theoretical values. Both mass and microanalysis were measured at Al-Azhar University in Nasr City, Cairo, Egypt. The purity of selected most actives compounds **5d** and **13c** was 97.46 and 98.99%, respectively, as determined by HPLC (Agilent Technologies, Santa Clara, CA). Ten µL of the solution was injected on a column (100 mm × 3.0 mm; 3.5 µm; ZORBAX® XDB-C18). The column was kept in a thermostat at 25 °C. Water and acetonitrile (60:40) were used as the mobile phase at flow rate of 1.50 mL/min operated at 254 nm. Retention time (min), area peak, and the purity percentage obtained from HPLC analysis are summarised in Tables S1 and S2 and Figures S58 and S59 (see Supporting information).

General procedure for preparation of compounds 3a–c

A mixture of isatin derivatives **2a–c** (0.3 mmol) in hot, dry methanol (10 mL) and a few drops of acetic acid (glacial) was added to an equimolar amount of compound **1** (112 mg, 0.3 mmol) in dry methanol (10 mL). The reaction mixture was heated under reflux for 24 h. To obtain the pure products, **3a–c**, the separated products were collected, washed with pet. ether, and recrystallised from isopropanol.

(E)-4-((4-(2-(5-Methyl-2-oxoindolin-3-ylidene)hydrazinyl)-6-(phenylamino)-1,3,5-triazin-2-yl)amino)benzenesulfonamide 3a. A yellow powder, yield: 63%. Mp: 275–277 °C. ^{1}H NMR (400 MHz, DMSO-d_6 and DMF) δ: 2.34 (s, 3H, CH_3), 6.84 (s, 1H, 7-H of isatin), 7.09 (s, 1H, 4-H of phenylamine), 7.22 (s, 1H, 6-H of isatin), 7.28 (s, 2H, SO_2NH_2), 7.36 (s, 2H, 3,5-H_2 of phenylamine), 7.76–7.96 (m, 5H, 2,6-H_2 of phenylamine, 4-H of isatin and 2,6-H_2 of benzenesulfonamide), 8.05 (s, 2H, 3,5-H_2 of benzenesulfonamide), 9.99 (s, 1H, 6-NH), 10.25 (s, 1H, 2-NH), 10.68 (s, 2H, 4-NH and CONH). ^{13}C NMR (100 MHz, DMSO-d_6 and DMF) δ: 21.22, 110.72, 116.51, 119.92, 121.44, 123.33, 126.79, 128.96, 130.88, 132.76, 137.59, 138.03, 139.80, 141.36, 143.36, 164.77, 165.41, 165.85. MS (ESI) (m/z): 515.53 [M^+]. Anal. calcd for $C_{24}H_{21}N_9O_3S$: C, 55.91, H, 4.11; N, 24.45; S, 6.22. Found: C, 55.60; H, 4.15; N, 24.38; S, 6.15.

(Z)-4-((4–(2-(5-Chloro-2-oxoindolin-3-ylidene)hydrazinyl)-6-(phenylamino)-1,3,5-triazin-2-yl)amino)benzenesulfonamide 3b. A yellow powder, yield: 74%. Mp: 299–300 °C. ^{1}H NMR (400 MHz, DMSO-d_6 and DMF) δ: 7.01 (d, 1H, 7-H of isatin, J = 8.0 Hz), 7.10 (t, 1H, 4-H of phenylamine, J = 7.6 Hz), 7.28 (s, 2H, SO_2NH_2), 7.37 (t, 2H, 3,5-H_2 of phenylamine, J = 7.6 Hz), 7.40 (d, 1H, 6-H of isatin, J = 8.0 Hz), 7.43 (s, 1H, 4-H of isatin), 7.75 (d, 2H, 2,6-H_2 of phenylamine, J = 7.6 Hz), 7.76 (s, 2H, 2,6-H_2 of benzenesulfonamide), 7.96 (s, 2H, 2,6-H_2 of benzenesulfonamide), 9.99 (s, 1H, 6-NH), 10.22 (s, 1H, 2-NH), 11.37 (s, 1H, CONH), 12.74 (s, 1H, 4-NH). ^{13}C NMR (100 MHz, DMSO-d_6 and DMF) δ: 113.12, 119.74, 119.96, 122.56, 126.82, 126.99, 128.98, 130.43, 133.07, 137.83, 140.67, 143.10, 163.40, 164.29, 164.88. MS (ESI) (*m/z*): 535.59 [M^+]. Anal. calcd for $C_{23}H_{18}ClN_9O_3S$: C, 51.54, H, 3.39; N, 23.52; S, 5.98. Found: C, 51.82; H, 3.36; N, 23.27; S, 6.13.

(E)-4-((4–(2-(1-Benzyl-5-chloro-2-oxoindolin-3-ylidene)hydrazinyl)-6-(phenylamino)-1,3,5-triazin-2-yl)amino)benzenesulfonamide 3c. A yellow powder, yield: 74%. Mp: 222–224 °C. ^{1}H NMR (500 MHz, DMSO-d_6) δ: 4.99 (s, 2H, CH_2), 7.02–7.08 (m, 2H, 7-H of isatin and 4-H of phenylamine), 7.25–7.45 (m, 10H, SO_2NH_2 and Ar-Hs), 7.71–8.08 (m, 7H, Ar-Hs), 9.97 (s, 1H, 6-NH), 10.23 (s, 1H, 2-NH), 11.15 (s, 1H, 4-NH). ^{13}C NMR (125 MHz, DMSO-d_6) δ: 42.73, 111.99, 119.21, 119.56, 121.62, 126.38, 127.22, 127.34, 127.59, 127.71, 128.55, 128.80, 135.54, 136.10, 137.24, 137.42, 140.43, 141.79, 142.75, 161.10, 163.55, 163.82, 164.41, 165.42. MS (ESI) (*m/z*): 625.88 [M^+]. Anal. calcd for $C_{30}H_{24}ClN_9O_3S$: C, 57.55, H, 3.86; N, 20.13; S, 5.12. Found: C, 57.20; H, 3.92; N, 20.29; S, 5.31.

General procedure for preparation of compounds 5a–d and 7a–e

In a round-bottomed flask (25 mL), the solution of compound **1** (112 mg, 0.3 mmol) in absolute methyl alcohol was added to an equimolar amount of the different substituted benzaldehyde derivatives **4a**–**c** or benzophenone **4d**, or different pyrazole-4-carbaldehydes **6a**–**e** in abs. methanol (5 mL) and a few drops of acetic acid (glacial). The mixture of reaction was heated under reflux for 5 h. The separated products were collected, washed with petroleum ether, and recrystallised from isopropanol to get the pure compounds **5a**–**d** and **7a**–**e**.

(E)-4-((4–(2-(4-(1H-Imidazol-1-yl)benzylidene)hydrazinyl)-6-(phenylamino)-1,3,5-triazin-2-yl)amino)benzenesulfonamide 5a. An off-white powder, yield: 81%. Mp: 217–219 °C. ^{1}H NMR (500 MHz, DMSO-d_6) δ: 7.02 (t, 1H, 4-H of phenylamine, $J = 7.5$ Hz), 7.14 (s, 1H, 4-H of imidazole), 7.23 (s, 2H, SO_2NH_2), 7.32 (t, 2H, 3,5-H_2 of phenylamine, $J = 7.5$ Hz), 7.71 (d, 2H, 2,6-H_2 of phenylamine, $J = 7.5$ Hz), 7.77 (d, 3H, 3,5-H_2 of phenyl and 5-H of imidazole, $J = 7.5$ Hz), 7.82 (*br*. s, 4H, 2,6-H_2 of phenyl and 2,6-H_2 of benzenesulfonamide), 8.02 (*br*. s, 2H, 3,5-H_2 of benzenesulfonamide), 8.24 (s, 1H, N = CH), (s, 1H, 2-H of imidazole), 9.41–9.86 (m, 2H, 2-NH and 6-NH), 11.16 (s, 1H, 4-NH). ^{13}C NMR (125 MHz, DMSO-d_6) δ: 117.93, 119.25, 120.48, 126.31, 127.93, 128.50, 130.08, 133.44, 135.58, 136.74, 137.30, 164.14. MS (ESI) (*m/z*): 526.95 [M^+]. Anal. calcd for $C_{25}H_{22}N_{10}O_2S$: C, 57.02; H, 4.21; N, 26.60; S, 6.09. Found: C, 57.40; H, 4.09; N, 26.46; S, 6.20.

(E)-4-((4-(2-(4-Morpholinobenzylidene)hydrazinyl)-6-(phenylamino)-1,3,5-triazin-2-yl)amino)benzenesulfonamide 5b. A pale green powder, yield: 77%. Mp: 278–280 °C. ^{1}H NMR (400 MHz, DMSO-d_6) δ: 3.21 (s, 4H, 2XCH_2 of morpholine), 3.76 (s, 4H, 2XCH_2 of morpholine), 7.03 (s, 3H, 4-H of phenylamine and 3,5-H_2 of phenyl), 7.29 (s, 4H, SO_2NH_2 and 3,5-H_2 of phenylamine), 7.60 (s, 2H, 2,6-H_2 of phenylamine), 7.77 (br. s, 4H, 2,6-H_2 of phenyl and 2,6-H_2 of benzenesulfonamide), 8.07 (s, 2H, 3,5-H_2 of benzenesulfonamide), 8.15 (s, 1H, N = CH), 9.38-9.88 (m, 2H, 6-NH and 2-NH), 10.92 (s, 1H, NH of 4-NH). APT ^{13}CNMR (100 MHz, DMSO-d_6) showed signals for CH appeared at the negative side (below the base line of the spectrum); 114.97, 119.57, 120.84, 122.64, 126.73, 128.18, 128.88, and 144.28 whereas CH_2, quaternary carbons and carbons of deuterated DMSO solvent were observed at positive side (above the base line of the spectrum); 48.11, 66.46, 125.77, 137.06, 140.38, 143.88, 152.21, and 164.36. MS (ESI) (*m/z*): 545.52 [M^+]. Anal. calcd for $C_{26}H_{27}N_9O_3S$: C, 57.23, H, 4.99; N, 23.10; S, 5.88. Found: C, 57.59; H, 5.09; N, 23.23; S, 5.99.

(E)-4-((4-(2-(3,5-Dibromo-4-hydroxybenzylidene)hydrazinyl)-6-(phenylamino)-1,3,5-triazin-2-yl)amino)benzenesulfonamide 5c. An off-white powder, yield: 70%. Mp: 225–227 °C. ^{1}H NMR (500 MHz, DMSO-d_6) δ: 7.03 (t, 1H, 4-H of phenylamine, $J = 8.0$ Hz), 7.24 (s, 2H, SO_2NH_2), 7.33 (s, 2H, 3,5-H_2 of phenylamine), 7.73–8.02 (m, 8H, Ar-Hs), 8.07 (s, 1H, N = CH), 9.49–9.93 (m, 2H, 2-NH and 6-NH), 10.37 (s, 1H, 4-NH), 11.36 (s, 1H, OH). ^{13}C NMR (125 MHz, DMSO-d_6) δ: 112.28, 118.94, 119.12, 119.38, 126.34, 128.49, 130.25, 132.25, 132.07, 137.00, 151.63, 163.79. MS (ESI) (*m/z*): 631.05 [M^+]. Anal. calcd for $C_{22}H_{18}Br_2N_8O_3S$: C, 41.66; H, 2.86; N, 17.67; S, 5.05. Found: C, 41.85; H, 2.98; N, 17.85; S, 5.12.

4-((4-(2-(Diphenylmethylene)hydrazinyl)-6-(phenylamino)-1,3,5-triazin-2-yl)amino)benzenesulfonamide 5d. An off-white powder, yield: 77%. Mp: 218–220 °C. HPLC analysis: retention time, 8.621 min; peak area, 97.46%. ^{1}H NMR (400 MHz, DMSO-d_6) δ: 7.05 (s, 1H, 4-H of phenylamine), 7.28 (s, 2H, SO_2NH_2), 7.3**3**–7.98 (m, 18H, Ar-Hs), 8.39 (s, 1H, N = CH), 9.67 (s, 1H, 6-NH) 9.94 (s, 1H, 2-NH). ^{13}C NMR (100 MHz, DMSO-d_6) δ: 119.65, 120.88, 122.92, 126.75, 126.82, 127.37, 128.89, 128.95, 129.03, 129.80, 130.09, 130.28, 132.27, 133.18, 137.39, 137.75, 140.09, 143.58, 164.29, 164.71. MS (ESI) (*m/z*): 536.39 [M^+]. Anal. calcd for $C_{28}H_{24}N_8O_2S$: C, 62.67, H, 4.51; N, 20.88; S, 5.97. Found: C, 62.90; H, 4.60; N, 20.58; S, 6.11.

(E)-4-((4-(2-((3-Phenyl-1H-pyrazol-4-yl)methylene)hydrazinyl)-6-(phenylamino)-1,3,5-triazin-2-yl)amino)benzenesulfonamide 7a. A white powder, yield: 76%. Mp: 258–260 °C. ^{1}H NMR (500 MHz, DMSO-d_6) δ: 6.99 (t, 1H, 4-H of phenylamine, $J = 7.5$ Hz), 7.22 (s, 2H, SO_2NH_2), 7.29 (t, 2H, 3,5-H_2 of phenylamine, $J = 7.5$ Hz), 7.48–8.09 (m, 12H, Ar-Hs), 8.30 (s, 1H, N = CH), 9.32–9.83 (m, 2H, 6-NH and 2-NH), 10.83 (s, 1H, 4-NH), 13.42 (s, 1H, NH of pyrazole). ^{13}C NMR (125 MHz, DMSO-d_6) δ: 114.45, 119.04, 120.25,122.12, 126.31, 128.14, 128.45, 128.71, 129.18, 136.52, 137.43, 141.66, 143.40, 163.78. MS (ESI) (*m/z*): 526.97 [M^+]. Anal. calcd for $C_{25}H_{22}N_{10}O_2S$: C, 57.02, H, 4.21; N, 26.60; S, 6.09. Found: C, 57.40; H, 4.11; N, 26.35; S, 6.29.

(E)-4-((4-(2-((1,3-Diphenyl-1H-pyrazol-4-yl)methylene)hydrazinyl)-6-(phenylamino)-1,3,5-triazin-2-yl)amino)benzenesulfonamide 7b. A buff powder, yield: 70%. Mp: 255–256 °C. ^{1}H NMR (500 MHz, DMSO-d_6) δ: 6.99–7.02 (m, 1H, 4-H of phenylamine), 7.21–7.27 (m, 2H, SO_2NH_2), 7.30 (t, 1H, Ar-H, $J = 7.5$ Hz), 7.38 (t, 2H, Ar-Hs, $J = 7.5$ Hz), 7.40–7.55 (m, 6H, Ar-Hs), 7.71–7.74 (m, 4H, Ar-Hs), 7.95–8.02 (m, 3H, Ar-Hs), 8.35 (s, 1H, N = CH), 8.67 (s, 1H, Ar-H), 8.76 (s, 1H, Ar-H), 9.16 (s, 1H, Ar-H), 9.47–9.92 (m, 2H, 6-NH and 2-NH), 10.99 (s, 1H, 4-NH). ^{13}C NMR (125 MHz, DMSO-d_6) δ: 116.46, 118.96, 127.27, 128.61, 128.82, 128.88, 129.71, 131.81, 138.94, 152.91, 153.58. MS (ESI) (*m/z*): 602.97 [M^+]. Anal. calcd for $C_{31}H_{26}N_{10}O_2S$: C, 61.78, H, 4.35; N, 23.24; S, 5.32. Found: C, 61.92; H, 4.40; N, 23.32; S, 5.53.

(E)-4-((4-(2-((3-(4-Chlorophenyl)-1-phenyl-1H-pyrazol-4-yl)methylene)hydrazinyl)-6-(phenylamino)-1,3,5-triazin-2-yl)amino)benzenesulfonamide 7c. A white powder, yield: 82%. Mp: 248–250 °C. ^{1}H NMR (500 MHz, DMSO-d_6) δ: 7.02 (t, 1H, 4-H of phenylamine, $J = 7.0$ Hz), 7.23 (s, 2H, SO_2NH_2), 7.31 (t, 2H, 3,5-H_2 of phenylamine, $J = 7.0$ Hz), 7.39 (t, 1H, Ar-H, $J = 7.0$ Hz), 7.55–7.60 (m, 4H, Ar-H), 7.70–7.81 (m, 6H, Ar-Hs), 7.96–8.01 (m, 4H, Ar-Hs), 8.34 (s, 1H, N = CH), 8.79 (s, 1H, Ar-H), 9.51–9.79 (m, 2H, 6-NH and 2-NH), 11.12 (s, 1H, 4-NH). ^{13}C NMR (125 MHz, DMSO-d_6) δ: 117.53, 118.78, 119.30, 126.36, 127.16, 128.53, 128.92, 129.83, 130.03, 131.00, 133.41, 139.04, 150.09. MS (ESI) (*m/z*): 636.70 [M^+]. Anal. calcd for $C_{31}H_{25}ClN_{10}O_2S$: C, 58.44, H, 3.96; N, 21.98; S, 5.03. Found: C, 58.25; H, 3.90; N, 22.22; S, 5.16.

(E)-4-((4-(2-((3-(4-Bromophenyl)-1-phenyl-1H-pyrazol-4-yl)methylene)hydrazinyl)-6-(phenylamino)-1,3,5-triazin-2-yl)amino)benzenesulfonamide 7d. An off-white powder, yield: 83%. Mp: 246–248 °C. ^{1}H NMR (500 MHz, DMSO-d_6) δ: 7.01 (t, 1H, 4-H of phenylamine, $J = 7.0$ Hz), 7.22 (s, 2H, SO_2NH_2), 7.30 (t, 2H, 3,5-H_2 of phenylamine, $J = 7.0$ Hz), 7.39 (t, 1H, Ar-H, $J = 7.0$ Hz), 7.56 (t, 2H, Ar-Hs, $J = 7.0$ Hz), 7.70–7.81 (m, 8H, Ar-Hs), 7.95–8.02 (m, 4H, Ar-Hs), 8.33 (s, 1H, N = CH), 8.79 (s, 1H, Ar-H), 9.47–9.86 (m, 2H, 6-NH and 2-NH), 11.02 (s, 1H, 4-NH). ^{13}C NMR (125 MHz, DMSO-d_6) δ: 117.57, 118.79, 119.19, 120.64, 122.05, 122.30, 126.34, 127.15, 128.49, 129.82, 130.30, 131.36, 131.82, 136.73, 139.04, 143.36, 150.11, 164.11. MS (ESI) (*m/z*): 680.98 [M^+]. Anal. calcd for $C_{31}H_{25}BrN_{10}O_2S$: C, 54.63, H, 3.70; N, 20.55; S, 4.70. Found: C, 54.90; H, 3.79; N, 20.73; S, 4.82.

(E)-4-((4-(2-((3-(4-Methoxyphenyl)-1-phenyl-1H-pyrazol-4-yl)methylene) hydrazinyl)-6-(phenylamino)-1,3,5-triazin-2-yl)amino)benzenesulfonamide 7e. An off-white powder, yield: 76%. Mp: 238–240 °C. ^{1}H NMR (500 MHz, DMSO-d_6) δ: 3.81 (s, 3H, OCH_3), 7.01 (t, 1H, 4-H of phenylamine, $J = 7.0$ Hz), 7.08 (d, 2H, Ar-Hs, $J = 9.0$ Hz), 7.23 (s, 2H, SO_2NH_2), 7.30 (t, 2H, 3,5-H_2 of phenylamine, $J = 7.0$ Hz), 7.37 (t, 1H, Ar-H, $J = 7.0$ Hz), 7.56 (t, 2H, Ar-Hs, $J = 7.0$ Hz), 7.66–7.81 (m, 6H, Ar-Hs), 7.94–8.01 (m, 4H, Ar-Hs), 8.33 (s, 1H, N = CH), 8.80 (s, 1H, Ar-H), 9.44-9.76 (m, 2H, 6-NH and 2-NH), 11.01 (s, 1H, 4-NH). ^{13}C NMR (125 MHz, DMSO-d_6) δ: 55.30, 114.28, 117.16, 118.63, 119.15, 124.51, 126.33, 126.87, 128.48, 129.60, 129.77, 139.15, 151.27, 159.59. MS (ESI) (*m/z*): 631.84 [M^+]. Anal. calcd for $C_{32}H_{28}N_{10}O_3S$: C, 60.75, H, 4.46; N, 22.14; S, 5.07. Found: C, 60.93; H, 4.57; N, 22.38; S, 5.18.

General procedure for preparation of compound 9

The mixture of compound **1** (112 mg, 0.3 mmol) and ethyl cyanoacetate (34 mg, 0.3 mmol) in acetic acid (glacial) (5 mL) was refluxed for 36 h. The mixture was filtered while hot. Then, it dried and crystallised from absolute ethanol.

4-((4-(5-Imino-3-oxopyrazolidin-1-yl)-6-(phenylamino)-1,3,5-triazin-2-yl)amino)benzenesulfonamide 9. A white powder, yield: 75%. Mp: 217–218 °C. ^{1}H NMR (400 MHz, DMSO-d_6) δ: 1.95 (s, 2H, CH_2 pyrazolidine), 7.01 (t, 1H, 4-H of phenylamine, $J = 7.2$ Hz), 7.23 (s, 2H, SO_2NH_2), 7.30 (s, 2H, 3,5-H_2 of phenylamine), 7.70 (d, 2H, 2,6-H_2 of phenylamine, $J = 8.0$ Hz), 7.79 (s, 2H, 2,6-H_2 of benzenesulfonamide), 8.00 (s, 2H, 3,5-H_2 of benzenesulfonamide), 8.99 (s, 1H, C = NH), 9.35-7.40 (m, 1H, 6-NH), 9.65–9.67 (m, 1H, 2-NH), 9.79 (s, 1H, CONH). ^{13}C NMR (100 MHz, DMSO-d_6) δ: 39.24 (masked by DMSO solvent), 119.46, 120.69, 122.60, 126.72, 128.86, 137.05, 140.31, 143.83, 164.50, 164.74, 167.76, 169.41. MS (ESI) (*m/z*): 438.99 [M^+]. Anal. calcd for $C_{18}H_{17}N_9O_3S$: C, 49.20, H, 3.90; N, 28.69; S, 7.30. Found: C, 49.52; H, 3.99; N, 28.96; S, 7.04.

General procedure for preparation of compounds 11a,b

Compound **1** (372 mg, 1 mmol), prop-2-en-1-ones **10a** or **10b** (1 mmol), and potassium hydroxide (50 mg, 1.25 mmol) were mixed and refluxed for 72 h in absolute methanol (10 mL). After adding HCl (2 N) to neutralise the reaction mixture in water, the residue was filtered out. The obtained crude products **11a,b** crystallised from isopropanol.

4-((4-(3,5-Bis(4-Chlorophenyl)-4,5-dihydro-1H-pyrazol-1-yl)-6-(phenylamino)-1,3,5-triazin-2-yl)amino)benzenesulfonamide 11a. A light brown powder, yield: 75%. Mp: 290–292 °C. ^{1}H NMR (400 MHz, DMSO-d_6) δ: 3.18 (d, 1H, 4-H of pyrazoline, $J = 16.8$ Hz), 3.92–3.99 (m, 1H, 4-H pyrazoline), 5.88 (s, 1H, 5-H pyrazoline), 7.0**0** (s, 1H, 4-H of phenylamine), 7.26–7.46 (m, 8H, SO_2NH_2, 3,5-H_2 of phenylamine and Ar-Hs), 7.58-8.13 (m, 10H, Ar-Hs), 9.45–9.79 (m, 2H, 6-NH and 2-NH). ^{13}C NMR (100 MHz, DMSO-d_6) δ: 42.28, 61.24, 119.49, 120.46, 122.57, 126.72, 127.56, 128.67, 128.85, 129.22, 129.42, 130.91, 132.13, 135.04, 137.19, 142.25, 153.20, 162.59, 164.4. MS (ESI) (*m/z*): 630.83 [M^+]. Anal. calcd for $C_{30}H_{24}Cl_2N_8O_2S$: C, 57.06, H, 3.83; N, 17.74; S, 5.08. Found: C, 57.35; H, 3.95; N, 17.99; S, 5.19.

4-((4-(5-(Benzo[d][1,3]dioxol-5-yl)-3-(4-chlorophenyl)-4,5-dihydro-1H-pyrazol-1-yl)-6-(phenylamino)-1,3,5-triazin-2-yl)amino)benzenesulfonamide 11b. A light brown powder, yield: 73%. Mp: 290–292 °C. ^{1}H NMR (400 MHz, DMSO-d_6) δ: 3.15 (d, 1H, 4-H pyrazoline, $J = 16.0$ Hz), 3.88–3.95 (m, 1H, 4-H pyrazoline), 5.80 (d, 1H, 5-H pyrazoline, $J = 16.0$ Hz), 5.99 (s, 2H, OCH_2O), 6.77 (s, 1H, Ar-H), 6.82 (s, 1H, Ar-H), 6.91–6.92 (m, 1H, Ar-H), 7.01 (s, 1H, Ar-H), 7.27 (br s, 4H, SO_2NH_2 and Ar-Hs), 7.46–8.13 (m, 10H, Ar-Hs), 9.45-9.94 (m, 2H, 6-NH and 2-NH). ^{13}C NMR (100 MHz, DMSO-d_6) δ: 42.53, 56.51, 101.50, 106.08, 108.91, 118.55, 119.43, 120.50, 122.55, 126.74, 128.63, 128.83, 129.40, 131.02, 134.97, 137.10, 137.30, 140.00, 143.69, 146.75, 148.04, 153.25, 162.61, 164.39. MS (ESI) (*m/z*): 640.56 [M^+]. Anal. calcd for $C_{31}H_{25}ClN_8O_4S$: C, 58.08, H, 3.93; N, 17.48; S, 5.00. Found: C, 58.33; H, 3.84; N, 17.84; S, 5.14.

General procedure for preparation of compounds 13a–e

The mixture of the compound **1** (372 mg, 1 mmol) and 1,3-diketones derivatives **12a**–**e** (1 mmol) in abs. methanol (5 mL) was refluxed for 5 h. The mixture was evaporated under a vacuum and refrigerated in cold water (20 mL) overnight. Products **13a**–**e** were filtered, dried, and recrystallised from petroleum ether.

4-((4-(3,5-Dimethyl-1H-pyrazol-1-yl)-6-(phenylamino)-1,3,5-triazin-2-yl)amino)benzenesulfonamide 13a. A buff powder, yield: 55%. Mp: 210–212 °C. ^{1}H NMR (400 MHz, DMSO-d_6) δ: 2.21 (s, 3H, CH_3 pyrazole), 2.66 (s, 3H, CH_3 pyrazole), 6.16 (s, 1H, 4-H pyrazole), 7.12 (t, 1H, 4-H of phenylamine, $J = 7.2$ Hz), 7.29 (s, 2H, SO_2NH_2), 7.38 (t, 2H, 3,5-Hs of phenylamine, $J = 7.2$ Hz), 7.76 (s, 4H, 2,6-Hs of phenylamine and benzenesulfonamide), 7.94 (s, 2H, 3,5-Hs of benzenesulfonamide), 10.12 (s, 1H, 6-NH), 10.35 (s, 1H, 2-NH). ^{13}C NMR (100 MHz, DMSO-d_6) δ: 13.93, 15.73, 110.72, 120.35, 122.08, 123.88, 126.82, 128.99, 138.12, 139.20, 142.84, 143.28, 150.47, 163.35, 165.02, 165.07. MS (ESI) (*m/z*): 436.41 [M^+]. Anal. calcd for $C_{20}H_{20}N_8O_2S$: C, 55.03, H, 4.62; N, 25.67; S, 7.34. Found: C, 55.35; H, 4.80; N, 25.90; S, 7.52.

4-((4-(5-Methyl-3-phenyl-1H-pyrazol-1-yl)-6-(phenylamino)-1,3,5-triazin-2-yl)amino)benzenesulfonamide 13b. A white powder, yield: 68%. Mp: 280–282 °C. ^{1}H NMR (400 MHz, DMSO-d_6) δ: 2.29 (s, 3H, CH_3 pyrazole), 6.52 (s, 1H, 4-H pyrazole), 6.99 (t, 3H, 3,4,5-H_3 of phenylamine, $J = 7.2$ Hz), 7.20–7.55 (m, 9H, SO_2NH_2, C_6H_5-pyrazole and 2,6-H_2 of phenylamine), 7.60–8.50 (m, 4H, 2,3,5,6-H_4 of benzenesulfonamide), 10.04 (d, 1H, 6-NH), 10.50 (d, 1H, 2-NH). ^{13}C NMR (100 MHz, DMSO-d_6) δ: 13.84, 110.86, 119.78, 120.52, 123.17, 126.72, 128.62, 128.85, 128.98, 129.26, 131.51, 137.91, 145.49, 150.64, 163.84, 164.87. MS (ESI) (*m/z*): 498.33 [M^+]. Anal. calcd for $C_{25}H_{22}N_8O_2S$: C, 60.23, H, 4.45; N, 22.48; S, 6.43. Found: C, 60.55; H, 4.60; N, 22.80; S, 6.30.

4-((4-(3,5-Diphenyl-1H-pyrazol-1-yl)-6-(phenylamino)-1,3,5-triazin-2-yl)amino)benzenesulfonamide 13c. A yellow powder, yield: 54%. Mp: 198–200 °C. HPLC analysis: retention time, 8.128 min; peak area, 98.99%. ^{1}H NMR (400 MHz, DMSO-d_6) δ: 7.02–7.99 (m, 22H, Ar-Hs), 9.47–9.92 (m, 2H, 6-NH and 2-NH). ^{13}C NMR (100 MHz, DMSO-d_6) δ: 108.03, 119.99, 120.76, 126.14, 126.75, 128.69, 129.10, 129.37, 131.23, 132.55, 138.12, 146.41, 152.56, 165.07. MS (ESI) (*m/z*): 560.70 [M^+]. Anal. calcd for $C_{30}H_{24}N_8O_2S$: C, 64.27, H, 4.32; N, 19.99; S, 5.72. Found: C, 64.60; H, 4.23; N, 19.73; S, 5.57.

4-((4-(3-Phenyl-5-(pyridin-2-yl)-1H-pyrazol-1-yl)-6-(phenylamino)-1,3,5-triazin-2-yl)amino)benzenesulfonamide 13d. A buff powder, yield: 62%. Mp: 225–227 °C. ^{1}H NMR (400 MHz, DMSO-d_6) δ: 7.28-8.61 (m, 21H, Ar-Hs), 9.69–9.95 (m, 2H, 6-NH, and 2-NH). ^{13}C NMR (100 MHz, DMSO-d_6) δ: 119.53, 120.15, 120.54, 122.74, 123.20, 126.72, 127.03, 128.86, 129.30, 130.54, 131.92, 137.26, 137.83, 149.71, 154.54, 160.97, 163.90. MS (ESI) (*m/z*): 561.33 [M^+]. Anal. calcd for $C_{29}H_{23}N_9O_2S$: C, 62.02, H, 4.13; N, 22.45; S, 5.71. Found: C, 62.29; H, 4.02; N, 22.22; S, 5.59.

4-((4-(3–(4-Chlorophenyl)-5-(pyridin-2-yl)-1H-pyrazol-1-yl)-6-(phenylamino)-1,3,5-triazin-2-yl)amino)benzenesulfonamide 13e. A red powder, yield: 59%. Mp: 268–270 °C. ^{1}H NMR (400 MHz, DMSO-d_6) δ: 7.10–8.44 (m, 20H, Ar-Hs), 9.93–10.16 (m, 2H, 6-NH, and 2-NH). ^{13}C NMR (100 MHz, DMSO-d_6) δ:120.03, 121.33, 126.83, 129.01, 137.95, 163.91, 166.76. MS (ESI) (*m/z*): 594.80[M^+]. Anal. calcd for $C_{29}H_{22}ClN_9O_2S$: C, 58.44, H, 3.72; N, 21.15; S, 5.38. Found: C, 58.19; H, 3.57; N, 21.33; S, 5.49.

General procedure for preparation of compounds 15a,b

The mixture of **1** (1 mmol, 0.176 g) and ethyl chloroformate (1 mmol, 0.109 g) (in case compound **15a**) or CS_2 (1 mmol, 0.1 ml) (in case compound **15 b**) in pyridine (2 mL) was refluxed for 16 h. The mixture was poured into cold water and then acidified using dil. hydrochloric acid. The formed precipitate was filtered, washed several times with cold water, dried, and recrystallised to give compounds **15a,b**.

4-((3-Hydroxy-7-(phenylamino)-[1, 2, 4]triazolo[4,3-a][1, 3, 5]triazin-5-yl)amino)benzenesulfonamide 15a. A white powder, yield: 55%. Mp: above 300 °C. ^{1}H NMR (400 MHz, DMSO-d_6) δ: 7.11-7.37 (m, 5H, Ar-Hs), 7.67–8.01 (m, 6H, Ar-Hs), 9.99 (br. s, 3H, 6-NH, 2-NH, and OH). ^{13}C NMR (100 MHz, DMSO-d_6) δ: 126.80, 129.01. MS (ESI) (*m/z*): 398.79 [M^+]. Anal. calcd for $C_{16}H_{14}N_8O_3S$: C, 48.24, H, 3.54; N, 28.13; S, 8.05. Found: C, 48.45; H, 3.65; N, 28.30; S, 8.22.

4-((3-Mercapto-7-(phenylamino)-[1, 2, 4]triazolo[4,3-a][1, 3, 5]triazin-5-yl)amino)benzenesulfonamide 15b. A yellow powder, yield: 71%. Mp: above 300 °C. ^{1}H NMR (400 MHz, DMSO-d_6) δ: For one isomer; 7.11 (s, 1H, 4-H of phenylamine), 7.28 (s, 2H, SO_2NH_2), 7.38 (t, 2H, 3,5-H_2 of phenylamine, $J = 7.6$ Hz), 7.70–7.85 (m, 6H, Ar-Hs), 10.02 (s, 1H, 6-NH), 10.24 (s, 1H, 2-NH), 14.20 (s, 1H, SH). For second isomer; 7.28 (s, 1H, 4-H of phenylamine), 7.44 (s, 2H, SO_2NH_2), 7.49 (t, 2H, 3,5-H_2 of phenylamine, $J = 7.6$ Hz), 7.90–8.05 (m, 6H, Ar-Hs), 12.58 (s, 1H, 6-NH), 12.78 (s, 1H, 2-NH), 14.20 (s, 1H, SH). ^{13}C NMR (100 MHz, DMSO-d_6) δ: For both isomers; 120.01, 120.64, 121.12, 121.62, 123.76, 124.53, 125.85, 126.96, 127.41, 129.13, 129.79, 136.26, 138.34, 139.23, 140.51, 142.60, 148.81, 149.77, 152.73, 152.86, 157.02, 157.27, 158.13, 158.50. MS (ESI) (*m/z*): 414.16 [M^+]. Anal. calcd for $C_{16}H_{14}N_8O_2S_2$: C, 46.37, H, 3.40; N, 27.04; S, 15.47. Found: C, 46.69; H, 3.32; N, 27.22; S, 15.60.

Biological evaluation

The comprehensive procedures of biological assays of the target sulphonamides series **I** (**3a–c, 5a–d**, and **7a–e**) and series **II** (**9, 11a,b, 13a–e,** and **15a,b**) are presented in the Supplementary materials, including; CA I, II, IX, and XII inhibition studies,[33] NCI-USA screening,[50,72] antiproliferative activities under hypoxic conditions,[73] toxicity towards normal human cells,[47] cell migration study,[48] colony formation assay,[49] apoptosis assay,[74] and cell cycle analysis.[75,76]

In silico studies

The comprehensive procedures of *in silico* studies of the representative target sulphonamides Series **I** and **II** were presented in the Supplementary materials, including; molecular docking analysis[77] and MD simulations.[64]

Acknowledgements

The authors would like to thank Faculty of Pharmacy, Tanta University for financial support and the Deanship of scientific research at Umm Al-Qura University for supporting this work by grant code (22UQU4290565DSR86).

Disclosure statement

No potential conflict of interest was reported by the author(s).

Funding

This work was supported by Faculty of Pharmacy, Tanta University, and the Deanship of scientific research at Umm Al-Qura University for supporting this work by grant code [22UQU4290565DSR86].

ORCID

Haytham O. Tawfik http://orcid.org/0000-0001-6455-5716
Amany Belal http://orcid.org/0000-0003-1045-0163
Mohammed A. S. Abourehab http://orcid.org/0000-0003-1348-6567
Andrea Angeli http://orcid.org/0000-0002-1470-7192
Claudiu T. Supuran http://orcid.org/0000-0003-4262-0323

References

1. Feng CY, Chen ZF, Pei LL, et al. Genome-wide identification, phylogeny, and expression analysis of the CA gene family in tomato. Biotechnol Biotechnol Equip. 2020;34(1):70–83.
2. Momayyezi M, McKown AD, Bell SC, Guy RD. Emerging roles for carbonic anhydrase in mesophyll conductance and photosynthesis. Plant J. 2020;101(4):831–844.
3. Güttler A, Eiselt Y, Funtan A, et al. Betulin sulfonamides as carbonic anhydrase inhibitors and anticancer agents in breast cancer cells. Int J Mol Sci. 2021;22(16):8808–8821.
4. Becker HM, Deitmer JW. Proton transport in cancer cells: the role of carbonic anhydrases. IJMS. 2021;22(6):3171.
5. Supuran CT, Scozzafava A. Carbonic anhydrases as targets for medicinal chemistry. Bioorg Med Chem. 2007;15(13):4336–4350.

6. Osmaniye D, Türkeş C, Demir Y, et al. Design, synthesis, and biological activity of novel dithiocarbamate-methylsulfonyl hybrids as carbonic anhydrase inhibitors. Arch Pharm . 2022;355(8):2200132–15.
7. Zhang C, Fang L, Wang X, et al. Oncolytic adenovirus-mediated expression of decorin facilitates CAIX-targeting CAR-T therapy against renal cell carcinoma. Mol Ther Oncolytics. 2022;24:14–25.,
8. Mahon BP, Pinard MA, McKenna R. Targeting carbonic anhydrase IX activity and expression. Molecules. 2015;20(2):2323–2348.
9. Pettersen EO, Ebbesen P, Gieling RG, et al. Targeting tumour hypoxia to prevent cancer metastasis. From biology, biosensing and technology to drug development: the METOXIA consortium. J Enzyme Inhib Med Chem. 2015;30(5):689–721.
10. Lee SH, Griffiths JR. How and why are cancers acidic? Carbonic anhydrase IX and the homeostatic control of tumour extracellular pH. Cancers. 2020;12(6):1616–1625.
11. Supuran CT. How many carbonic anhydrase inhibition mechanisms exist? J Enzyme Inhib Med Chem. 2016;31(3):345–360.
12. Carta F, Vullo D, Osman SM, et al. Synthesis and carbonic anhydrase inhibition of a series of SLC-0111 analogs. Bioorg Med Chem. 2017;25(9):2569–2576.
13. Said MA, Eldehna WM, Nocentini A, et al. Sulfonamide-based ring-fused analogues for CAN508 as novel carbonic anhydrase inhibitors endowed with antitumor activity: design, synthesis, and in vitro biological evaluation. Eur J Med Chem. 2020;189:112019.,
14. Katariya KD, Shah SR, Reddy D. Anticancer, antimicrobial activities of quinoline based hydrazone analogues: synthesis, characterization and molecular docking. Bioorg Chem. 2020;94:1–14.
15. Goff GL, Ouazzani J. Natural hydrazine-containing compounds: biosynthesis, isolation, biological activities and synthesis. Bioorg Med Chem. 2014;22(23):6529–6544.
16. Alaa A-M, El-Azab AS, El-Enin MAA, et al. Synthesis of novel isoindoline-1, 3-dione-based oximes and benzenesulfonamide hydrazones as selective inhibitors of the tumor-associated carbonic anhydrase IX. Bioorg Chem. 2018;80:706–713.
17. Queen A, Khan P, Idrees D, et al. Biological evaluation of p-toluene sulphonylhydrazone as carbonic anhydrase IX inhibitors: an approach to fight hypoxia-induced tumors. Int J Biol Macromol. 2018;106:840–850.
18. Rodrigues T, da Cruz FP, Lafuente-Monasterio MJ, et al. Quinolin-4 (1 H)-imines are potent antiplasmodial drugs targeting the liver stage of malaria. J Med Chem. 2013;56(11):4811–4815.
19. Ressurreição AS, Gonçalves D, Sitoe AR, et al. Structural optimization of quinolon-4 (1 H)-imines as dual-stage antimalarials: toward increased potency and metabolic stability. J Med Chem. 2013;56(19):7679–7690.
20. Abo-Ashour MF, Eldehna WM, Nocentini A, et al. 3-Hydrazinoisatin-based benzenesulfonamides as novel carbonic anhydrase inhibitors endowed with anticancer activity: synthesis, in vitro biological evaluation and in silico insights. Eur J Med Chem. 2019;184:111768.
21. Eldeeb AH, Abo-Ashour MF, Angeli A, et al. Novel benzenesulfonamides aryl and arylsulfone conjugates adopting tail/dual tail approaches: synthesis, carbonic anhydrase inhibitory activity and molecular modeling studies. Eur J Med Chem. 2021;221:113486–12.
22. Chandak N, Ceruso M, Supuran CT, Sharma PK. Novel sulfonamide bearing coumarin scaffolds as selective inhibitors of tumor associated carbonic anhydrase isoforms IX and XII. Bioorg Med Chem. 2016;24(13):2882–2886.
23. Alaa A-M, El-Azab AS, Bua S, et al. Design, synthesis, and carbonic anhydrase inhibition activity of benzenesulfonamide-linked novel pyrazoline derivatives. Bioorg Chem. 2019;87:425–431.
24. Yamali C, Gul HI, Ozli G, et al. Exploring of tumor-associated carbonic anhydrase isoenzyme IX and XII inhibitory effects and cytotoxicities of the novel N-aryl-1-(4-sulfamoylphenyl)-5-(thiophen-2-yl)-1H-pyrazole-3-carboxamides. Bioorg Chem. 2021;115:105194–11.
25. Said MA, Eldehna WM, Nocentini A, et al. Synthesis, biological and molecular dynamics investigations with a series of triazolopyrimidine/triazole-based benzenesulfonamides as novel carbonic anhydrase inhibitors. Eur J Med Chem. 2020;185:111843–13.
26. Tawfik HO, Petreni A, Supuran CT, El-Hamamsy MH. Discovery of new carbonic anhydrase IX inhibitors as anticancer agents by toning the hydrophobic and hydrophilic rims of the active site to encounter the dual-tail approach. Eur J Med Chem. 2022;232:114190–21.
27. Jakusová K, Gáplovský M, Donovalová J, et al. Effect of reactants' concentration on the ratio and yield of E, Z isomers of isatin-3-(4-phenyl) semicarbazone and N-methylisatin-3-(4-phenyl) semicarbazone. Chem Paper. 2013;67(1):117–126.
28. Ghorab MM, Alsaid MS, Soliman AM, Ragab FA. VEGFR-2 inhibitors and apoptosis inducers: synthesis and molecular design of new benzo [g] quinazolin bearing benzenesulfonamide moiety. J Enzyme Inhib Med Chem. 2017;32(1):893–907.
29. Sharma PK, Balwani S, Mathur D, et al. Synthesis and anti-inflammatory activity evaluation of novel triazolyl-isatin hybrids. J Enzyme Inhib Med Chem. 2016;31(6):1520–1526.
30. AboulWafa OM, Daabees HM, Badawi WA. 2-Anilinopyrimidine derivatives: design, synthesis, in vitro antiproliferative activity, EGFR and ARO inhibitory activity, cell cycle analysis and molecular docking study. Bioorg Chem. 2020;99:103798–19.
31. Salem MS, Sakr SI, El-Senousy WM, Madkour HM. Synthesis, antibacterial, and antiviral evaluation of new heterocycles containing the pyridine moiety. Arch Pharm (Weinheim)). 2013;346(10):766–773.
32. Othman IMM, Gad-Elkareem MAM, Anouar EH, et al. Novel fused pyridine derivatives containing pyrimidine moiety as prospective tyrosyl-tRNA synthetase inhibitors: design, synthesis, pharmacokinetics and molecular docking studies. J Mol Struct. 2020;1219:128651.
33. George RF, Said MF, Bua S, Supuran CT. Synthesis and selective inhibitory effects of some 2-oxindole benzenesulfonamide conjugates on human carbonic anhydrase isoforms CA I, CA II, CA IX and CAXII. Bioorg Chem. 2020;95:103514.
34. Ghorab MM, Alsaid MS, Ceruso M, et al. Carbonic anhydrase inhibitors: synthesis, molecular docking, cytotoxic and inhibition of the human carbonic anhydrase isoforms I, II, IX, XII with novel benzenesulfonamides incorporating pyrrole, pyrrolopyrimidine and fused pyrrolopyrimidine moieties. Bioorg Med Chem. 2014;22(14):3684–3695.
35. Eldehna WM, Abo-Ashour MF, Nocentini A, et al. Enhancement of the tail hydrophobic interactions within the carbonic anhydrase IX active site via structural extension: Design and synthesis of novel N-substituted isatins-SLC-0111

hybrids as carbonic anhydrase inhibitors and antitumor agents. Eur J Med Chem. 2019;162:147–160.
36. Nocentini A, Trallori E, Singh S, et al. 4-Hydroxy-3-nitro-5-ureido-benzenesulfonamides selectively target the tumor-associated carbonic anhydrase isoforms IX and XII showing hypoxia-enhanced antiproliferative profiles. J Med Chem. 2018;61(23):10860–10874.
37. Demir-Yazı cı K, Bua S, Akgüneş NM, et al. Indole-based hydrazones containing A sulfonamide moiety as selective inhibitors of tumor-associated human carbonic anhydrase isoforms IX and XII. Int J Mol Sci. 2019;20:1–14.
38. Shaldam M, Nocentini A, Elsayed ZM, et al. Development of novel quinoline-based sulfonamides as selective cancer-associated carbonic anhydrase isoform IX inhibitors. Int J Mol Sci. 2021;22(20):11119–16.
39. Aggarwal M, Kondeti B, McKenna R. Insights towards sulfonamide drug specificity in α-carbonic anhydrases. Bioorg Med Chem. 2013;21(6):1526–1533.
40. Pinard MA, Boone CD, Rife BD, et al. Structural study of interaction between brinzolamide and dorzolamide inhibition of human carbonic anhydrases. Bioorg Med Chem. 2013;21(22):7210–7215.
41. Boyd MR, Paull KD. Some practical considerations and applications of the National Cancer Institute in vitro anticancer drug discovery screen. Drug Dev Res. 1995;34(2):91–109.
42. Rashid M, Husain A, Mishra R, et al. Design and synthesis of benzimidazoles containing substituted oxadiazole, thiadiazole and triazolo-thiadiazines as a source of new anticancer agents. Arab J Chem. 2019;12(8):3202–3224.
43. Singla P, Luxami V, Paul K. Synthesis and in vitro evaluation of novel triazine analogues as anticancer agents and their interaction studies with bovine serum albumin. Eur J Med Chem. 2016;117:59–69.
44. Acton EM, Narayanan VL, Risbood PA, et al. Anticancer specificity of some ellipticinium salts against human brain tumors in vitro. J Med Chem. 1994;37(14):2185–2189.
45. Al-Saadi MS, Rostom SA, HM. Faidallah 3-Methyl-2-(4-substituted phenyl)-4, 5-dihydronaphtho [1, 2-c]-pyrazoles: synthesis and inivitro biological evaluation as antitumour agents. Arch Pharm (Weinheim). 2008;341(3):181–190.
46. Krymov SK, Scherbakov AM, Salnikova DI, et al. Synthesis, biological evaluation, and in silico studies of potential activators of apoptosis and carbonic anhydrase inhibitors on isatin-5-sulfonamide scaffold. Eur J Med Chem. 2022;228:113997.
47. An B, Liu J, Fan Y, et al. Novel third-generation pyrimidines-based EGFR tyrosine kinase inhibitors targeting EGFR T790M mutation in advanced non-small cell lung cancer. Bioorg Chem. 2022;122:105743–14.
48. Hassan RA, Hamed MI, Abdou AM, El-Dash Y. Novel antiproliferative agents bearing substituted thieno [2, 3-d] pyrimidine scaffold as dual VEGFR-2 and BRAF kinases inhibitors and apoptosis inducers; design, synthesis and molecular docking. Bioorg Chem. 2022;125:105861–19.
49. Kadagathur M, Sujat Shaikh A, Panda B, et al. Synthesis of indolo/pyrroloazepinone-oxindoles as potential cytotoxic, DNA-intercalating and topo I inhibitors. Bioorg Chem. 2022;122:105706–105716.
50. Abdel-Aziz AA-M, El-Azab AS, AlSaif NA, et al. Synthesis, potential antitumor activity, cell cycle analysis, and multitarget mechanisms of novel hydrazones incorporating a 4-methylsulfonylbenzene scaffold: a molecular docking study. J Enzyme Inhib Med Chem. 2021;36(1):1521–1539.
51. Pfeffer CM, Singh AT. Apoptosis: a target for anticancer therapy. Int J Mol Sci. 2018;19:1–10.
52. Vermes I, Haanen C, Steffens-Nakken H, Reutelingsperger C. A novel assay for apoptosis flow cytometric detection of phosphatidylserine expression on early apoptotic cells using fluorescein labelled annexin V. J Immunol Methods. 1995;184(1):39–51.
53. Abdelrahman MA, Eldehna WM, Nocentini A, et al. Novel diamide-based benzenesulfonamides as selective carbonic anhydrase IX inhibitors endowed with antitumor activity: synthesis, biological evaluation and in silico insights. Int J Mol Sci. 2019;20:1–16.
54. Qin JL, Shen WY, Chen ZF, et al. Oxoaporphine metal complexes (Co II, Ni II, Zn II) with high antitumor activity by inducing mitochondria-mediated apoptosis and S-phase arrest in HepG2. Sci. Rep. 2017;7:1–18.
55. Zhong S, Li YG, Ji DF, et al. Protocatechualdehyde induces S-phase arrest and apoptosis by stimulating the p27KIP1-cyclin A/D1-CDK2 and mitochondrial apoptotic pathways in HT-29 Cells. Molecules. 2016;21(7):934–121.
56. Musa MA, Gbadebo AJ, Latinwo LM, Badisa VL. 7, 8-Dihydroxy-3-(4-nitrophenyl) coumarin induces cell death via reactive oxygen species–independent S-phase cell arrest. J. Biochem. Mol. Toxicol. 2018;32:794–801.
57. Nemr MT, AboulMagd AM, Hassan HM, et al. Design, synthesis and mechanistic study of new benzenesulfonamide derivatives as anticancer and antimicrobial agents via carbonic anhydrase IX inhibition. RSC Adv. 2021;11(42):26241–26257.
58. Dawood DH, Srour AM, Saleh DO, et al. New pyridine and chromene scaffolds as potent vasorelaxant and anticancer agents. RSC Adv. 2021;11(47):29441–29452.
59. Kim KH, Sederstrom JM. Assaying cell cycle status using flow cytometry. Curr Protoc Mol Biol. 2015;111:1–11.
60. Cvijetić IN, Tanç M, Juranić IO, et al. 5-Aryl-1H-pyrazole-3-carboxylic acids as selective inhibitors of human carbonic anhydrases IX and XII. Bioorg Med Chem. 2015;23(15):4649–4659.
61. Supuran CT. Multitargeting approaches involving carbonic anhydrase inhibitors: hybrid drugs against a variety of disorders. J Enzyme Inhib Med Chem. 2021;36(1):1702–1714.
62. Malebari AM, Ibrahim TS, Salem IM, et al. The anticancer activity for the bumetanide-based analogs via targeting the tumor-associated membrane-bound human carbonic anhydrase-IX enzyme. Pharmaceuticals. 2020;13(9):252–220.
63. Supuran CT, Scozzafava A. Carbonic anhydrase inhibitors: aromatic sulfonamides and disulfonamides act as efficient tumor growth inhibitors. J Enzyme Inhib. 2000;15(6):597–610.
64. Yousef RG, Ibrahim A, Khalifa MM, et al. Discovery of new nicotinamides as apoptotic VEGFR-2 inhibitors: virtual screening, synthesis, anti-proliferative, immunomodulatory, ADMET, toxicity, and molecular dynamic simulation studies. J Enzyme Inhib Med Chem. 2022;37(1):1389–1403.
65. Elrazaz EZ, Serya RA, Ismail NS, et al. Discovery of potent thieno [2, 3-d] pyrimidine VEGFR-2 inhibitors: design, synthesis and enzyme inhibitory evaluation supported by molecular dynamics simulations. Bioorg Chem. 2021;113:105019–16.
66. Belhassan A, Zaki H, Chtita S, et al. Camphor, artemisinin and sumac phytochemicals as inhibitors against COVID-19:

computational approach. Comput Biol Med. 2021;136:104758–17.
67. Guterres H, Im W. Improving protein-ligand docking results with high-throughput molecular dynamics simulations. J Chem Inf Model. 2020;60(4):2189–2198.
68. Jena AB, Kanungo N, Nayak V, et al. Catechin and curcumin interact with S protein of SARS-CoV2 and ACE2 of human cell membrane: insights from computational studies. Sci Rep. 2021;11(1):14.
69. Ali A, Ali A, Warsi MH, et al. Toward the discovery of a novel class of leads for high altitude disorders by virtual screening and molecular dynamics approaches targeting carbonic anhydrase. Int J Mol Sci. 2022;23(9):5054.
70. Costa RA, Rocha JA, Pinheiro AS, et al. A computational approach applied to the study of potential allosteric inhibitors protease NS2B/NS3 from dengue virus. Molecules. 2022;27(13):4118–4120.
71. Lee S, Wong AR, Yang AWH, Hung A. Interaction of compounds derived from the Chinese medicinal formula Huangqi Guizhi Wuwu Tang with stroke-related numbness and weakness targets: an in-silico docking and molecular dynamics study. Comput Biol Med. 2022;146:105568–105569.
72. Abdel-Aziz AAM, El-Azab AS, Alanazi AM, et al. Synthesis and potential antitumor activity of 7-(4-substituted piperazin-1-yl)-4-oxoquinolines based on ciprofloxacin and norfloxacin scaffolds: in silico studies. J Enzyme Inhib Med Chem. 2016;31(5):796–809.
73. Mussi S, Rezzola S, Chiodelli P, et al. Antiproliferative effects of sulphonamide carbonic anhydrase inhibitors C18, SLC-0111 and acetazolamide on bladder, glioblastoma and pancreatic cancer cell lines. J Enzyme Inhib Med Chem. 2022;37(1):280–286.
74. Eldehna WM, Abo-Ashour MF, Ibrahim HS, et al. Novel [(3-indolylmethylene) hydrazono] indolin-2-ones as apoptotic anti-proliferative agents: design, synthesis and in vitro biological evaluation. J Enzyme Inhib Med Chem. 2018;33(1):686–700.
75. Said MA, Eldehna WM, Nocentini A, et al. Sulfonamide-based ring-fused analogues for CAN508 as novel carbonic anhydrase inhibitors endowed with antitumor activity: design, synthesis, and in vitro biological evaluation. Eur. J. Med. Chem. 2020;189:1–14.
76. Eldehna WM, El-Naggar DH, Hamed AR, et al. One-pot three-component synthesis of novel spirooxindoles with potential cytotoxic activity against triple-negative breast cancer MDA-MB-231 cells. J Enzyme Inhib Med Chem. 2018;33(1):309–318.
77. Ewies EF, Sabry E, Bekheit MS, et al. Click chemistry-based synthesis of new benzenesulfonamide derivatives bearing triazole ring as selective carbonic anhydrase II inhibitors. Drug Dev Res . 2022;83(6):1281–1291.